REVIEW AND ANALYSIS OF HIGH VELOCITY IMPACT DATA

E. P. Bruce

General Electric Company
Missile and Space Vehicle Department
Philadelphia, Pennsylvania

AF 04 (647) 269

ABSTRACT

A thorough review ~~has been~~ was made of existing experimental data applicable to the impact of high velocity projectiles with semi-infinite metal targets. Empirical equations relating depth of penetration and crater volume to properties of the projectile and target ~~have been~~ were derived based upon the assumptions that:

1) projectile shape does not affect crater shape for projectiles which range from spheres to cylinders up to one caliber in length, and

2) craters are hemispherical.

Both of these assumptions are supported by the available data. Additional data and/or a rigorous theoretical treatment of the problem are required to evaluate the utility of the equations at higher impact velocities.

SYMBOLS

P_C - depth of penetration, measured from the plane of the undamaged target surface to the deepest point in the crater.

D_C - crater diameter, measured in the plane of the undamaged target surface.

$D_{C\ MAJ}$ - crater diameter, used only in describing craters formed under oblique impact, measured in the plane of the undamaged target surface and in-line with the projectile trajectory.

$D_{C\ MIN.}$ - crater diameter, used only in describing craters formed under oblique impact, measured in the plane of the undamaged target surface and normal to the projectile trajectory.

V_C - crater volume, measured to the plane of the undamaged target surface.

V_P - projectile volume.

ρ_P projectile mass density

ρ_T target mass density

v - impact velocity, measured normal to the target surface for impact at either normal or oblique incidence.

c - velocity of propagation of a plane longitudinal wave in a slender rod.

D - diameter of a cylindrical projectile

L - length or height of cylindrical projectile

D_S - diameter of a spherical projectile or diameter of a sphere having the same mass as a cylindrical projectile

θ - incidence angle in oblique impact, measured from the normal to the target surface to the projectile trajectory.

INTRODUCTION

Early in 1960, a review of existing single particle metal-to-metal impact data was initiated at the General Electric Missile and Space Vehicle Department.* The reasons for this review were threefold. First, the available data and analysis indicated that a uniform crater shape, that of a hemisphere, was approached as the impact velocity increased; second, the available, general, empirical relations for depth of penetration and crater volume were based on only a small portion of the existing data; and third, the existing relations for depth of penetration and crater volume, while based on separate analyses of penetration and volume data, did not yield a compatible set of equations. Specific reference is made to the following equations[1]

$$\frac{P_c}{D_s} = 2.28 \left(\frac{\rho_p}{\rho_T}\right)^{2/3} \left(\frac{v}{c}\right)^{2/3} \qquad (1)$$

$$\frac{V_c}{V_p} = 34 \left(\frac{\rho_p}{\rho_T}\right)^{3/2} \left(\frac{v}{c}\right)^{2} \qquad (2)$$

which were, at the time this study was initiated, the latest and most generally applicable relations in the field. If the assumption is made that for sufficiently high impact velocities only hemispherical craters will appear, then the penetration parameter (P_c/D_s) and

---

* This work was supported by the United States Air Force Ballistic Systems Division under Contract Number AF 04-(647)-269.

the crater volume parameter $\left(V_c/V_p\right)$ are related, from geometrical considerations alone, by

$$\frac{V_c}{V_p} = 4\left(\frac{P_c}{D_s}\right)^3 \qquad (3)$$

Examination of Equations 1 and 2 shows that they disagree with the requirements of Equation 3 both in the value of the numerical constants and in the exponents to which the quantity $\left(\rho_p/\rho_t\right)$ is raised. Consequently, the available data were examined to determine the projectile-target systems for which hemispherical craters had been observed. A $\pm$ 20% limitation on $\left(P_c/D_c\right)$ was selected, that is, only penetration and volume data in the velocity range where $\left(P_c/D_c\right)$ had reached and remained within the limits $0.4 \leq \left(P_c/D_c\right) \leq 0.6$ as the impact velocity was increased were considered. For these selected cases, a method of analysis similar to that used by Huth, et al[2], Charters and Locke[3], and Summers[1] was utilized. Specifically, the penetration and crater volume data were examined to ascertain whether equations of the same form as Equations 1 and 2 would result which would, at the same time, satisfy Equation 3. In order to incorporate data obtained as a result of impact investigations in which non-spherical projectiles were used, the diameter of a sphere having the same mass as the non-spherical projectile was calculated for these data and used in determining the penetration parameter $\left(P_c/D_s\right)$. Kineke's investigations with cylindrical projectiles of varying fineness ratio[4] form the basis for this step. Midway through this analysis, the data presented at the 1960 Hypervelocity Impact Symposium by

Kineke[5], Atkins[6], and Maiden[7] were included in this review. These data represent a large percentage of the available high velocity data.**

IMPACT AT NORMAL INCIDENCE

The sections that follow are devoted to the presentation and analysis of impact data. Detailed information describing projectile material, size, and shape; target material; projectile and target material properties; and parameters of interest with respect to the projectile-target system are presented in Table I. Material properties have been taken from handbooks in all cases where they were not presented in the data source.

Crater Profile

Data illustrating the variation of (P_c/D_c), the ratio of crater depth to crater diameter, with impact velocity are shown in Figures 1-7 for projectile-target systems in which projectiles of various materials have been impacted against targets of aluminum alloy, zinc, tin, steel, cadmium, copper, and lead. The low velocity peaks in the parameter (P_c/D_c), which occur only in certain systems, are associated with undeformed projectile penetration. The higher velocities required to produce projectile shatter also produce increasing degrees of flow in the target with the net result that even though penetration is increasing (cases have been observed where penetration initially drops off with the onset of projectile shatter[1]) a larger increase in crater diameter is taking place due to the dissipation of momentum in the target. Examination of the lead target data indicates that both the

** The author wishes to take this opportunity to thank Mr. John H. Kineke, Jr. of BRL, Mr. Walter W. Atkins of NRL, and Dr. C. J. Maiden formerly of CARDE for their cooperation in making their data available for this study.

presence and amplitude of the low velocity peak depends upon some function of the relative projectile-target densities and strengths. The tungsten carbide-lead system exhibits the highest peak -- tungsten carbide is both stronger and more dense than lead. However, both steel and copper exhibit peaks while 2024 - T3 aluminum does not -- all are less dense and stronger than lead.

The data show, however, that as the impact velocity increases, the crater profile parameter $\left(P_c/D_c\right)$ approaches 0.5, the value corresponding to hemispherical craters. The velocity at which this level is reached can be quite high, particularly for cases in which either strong heavy or strong light projectiles impact against a strong target as illustrated by the data for tungsten carbide and 2024 - T3 aluminum impacting steel (Figure 4). It is of interest to note that the $\left(P_c/D_c\right) = 0.5$ level is, in general, reached at a relatively low velocity for systems in which the projectile and target are of identical materials. The data for the aluminum projectile - 1100F aluminum target system (Figure 1) also indicates that small differences in material densities do not alter this observation.

Depth of Penetration

The penetration data for all projectile - target systems which have reached and maintained a value of $\left(P_c/D_c\right)$ within the established $\pm$ 20% tolerance are shown in Figures 8-14. These data, as presented, describe the variation of penetration in sphere diameters with the non-dimensional velocity parameter $\left(U/a\right)$. The data have been arranged in the order of increasing target density and subdivided to reflect effects due to

increases in projectile density for constant target density. The vertical line shown on each figure separates the data for which (P_c/D_c) is within $\pm$ 20% of 0.5 from the higher velocity data -- only data to the right of this line have been used in this analysis. These data have been analyzed, by a modified least squares technique, to determine the constant K_1 in the following relation:

$$\frac{P_c}{D_s} = K_1 \left(\frac{\nu}{c}\right)^{2/3} \qquad (4)$$

Normal least squares fitting procedures would result in determination of both the constant K_1 and the exponent; however, the exponent was fixed in this analysis since it had been established in a number of separate investigations.[1,5,6] The values of K_1 thus determined are presented in Table I.

The penetration data for the 2024 - T3 and T4 aluminum, steel, and copper systems in which the projectile and target materials were identical (Figures 8b, 11, and 13c respectively) and for the 2024 - T3 and T4 aluminum projectile-copper target system (Figure 13a) illustrate systems in which the (P_c/D_c) = 0.5 level is reached either at relatively low velocities and maintained throughout the velocity range or by a build-up from values less than 0.5. For these systems, the variation with $(\nu/c)^{2/3}$ is reached by a smooth transition after a higher power dependence. The penetration data for the following systems illustrate cases in which the (P_c/D_c) = 0.5 level is reached following low velocity undeformed projectile penetration in which much higher values of (P_c/D_c) are attained. steel projectiles-copper targets

(Figure 14b), and copper projectiles-lead targets (Figure 14c). For these cases the variation of (P_c/D_s) with $(v/c)^{2/3}$ is reached after a similar higher power dependence followed by a region in which penetration decreases and then increases. No effort has been expended in trying to define a minimum velocity at which $(v/c)^{2/3}$ dependence will appear for a given system. The two types of build up to this dependence are of primary interest in low velocity applications, however, the rather complete picture thus afforded illustrates that, for many systems, the highest velocities recorded were barely sufficient to yield impacts that produced the characteristic high velocity crater shape.

Crater Volume

The crater volume data, presented and ordered in a manner similar to that used with the penetration data, are shown in Figures 15-21. These data have also been analyzed by the modified least square technique to determine the constant K_2 in the relation

$$\frac{V_c}{V_p} = K_2 \left(\frac{v}{c}\right)^2 \qquad (5)$$

The exponent was fixed as shown in Equation 5 based upon the results of a number of independent investigations[1,5,6,7] many of which included portions of the total body of data included in this analysis. The values thus obtained for K_2 are tabulated in Table I.

The volume data do not reflect the changing nature of the parameter (P_c/D_c) as strongly as do the penetration data. The crater volume data at low velocities in systems that reach the $(P_c/D_c) = 0.5$ level

either at relatively low velocities and maintain it throughout the velocity range or by a build-up from values less than 0.5 (Figures 15, 17-19, 20a, 20c, 21a, and 21d) show very slight, if any, deviations from the established high velocity variation. However, for every system in which (ρ_c/D_c) has peaked at a value above 0.5 at low velocities and has reached 0.5 from above at higher velocities, a definite shift is present in the volume data that is associated with the transition to high velocity cratering after projectile shatter occurs. In every case the shift is toward lower high velocity values of (V_c/V_p) than would be estimated based upon an extrapolation of low velocity data. This characteristic behavior is illustrated by the following projectile-target systems: steel-copper (Figure 20b), steel-lead (Figure 21b), and copper-lead (Figure 21c).

Effect of Projectile and Target Density

The penetration and crater volume data for systems in which zinc, copper, and lead were used as targets indicate, by increases in K_1 and K_2 which correspond to increases in projectile density (see Table I) that penetration and crater volume are functions of projectile density. The data also indicate, for systems in which aluminum, steel and copper were used as projectiles, that penetration and crater volume are also functions of target density. The crater volume (K_2) data have been plotted versus target density (for constant projectile density families) and versus projectile density (for constant target density families), as shown in Figures 22 and 23. The results of previous investigations[1,7] indicate that K_2 should be proportional to

$(\rho_T)^{-3/2}$ and to $(\rho_p)^{3/2}$. Accordingly, lines representing this variation have been drawn through the data for each family in Figures 22 and 23. The data exhibit some scatter; but in general, they substantiate the previous results. The penetration data (K_1) permit an independent check on these observations, since, if these data satisfy Equation 3, then K_1 should be proportional to $(\rho_T)^{-1/2}$ and to $(\rho_p)^{1/2}$. The penetration data are presented in Figures 24 and 25, along with lines which describe the above variation for each family. The proposed variation adequately describes the actual variation, indicating compatibility between the penetration and crater volume data as required by Equation 3.

Correlation of All Data

The step remaining in the establishment of general penetration and crater volume equations requires a determination of the constants of proportionality in the relations

$$\frac{P}{D_s} = K_3 \left(\frac{\rho_p}{\rho_T}\right)^{1/2} \left(\frac{v}{c}\right)^{2/3} \qquad (6)$$

and

$$\frac{V_c}{V_p} = K_4 \left(\frac{\rho_p}{\rho_T}\right)^{3/2} \left(\frac{v}{c}\right)^{2} \qquad (7)$$

Equation 3 again provides a check between the two sets of data, since it requires that $K_4 = 4\ (K_3)^3$. The values of K_3 and K_4 determined by averaging over the complete body of data, thereby giving the data from each projectile-target system equal weight, are: $K_3 = 2.01$, and $K_4 = 30.25$. The agreement between the sets of data is again satisfactory, since $\sqrt[3]{\frac{K_4}{4}} = 1.96$. The following general equations, which

satisfy Equation 3, thus result for high velocity cratering in semi-infinite, ductile metal targets:

$$\frac{P_c}{D_s} = 1.96 \left(\frac{\rho_p}{\rho_T}\right)^{1/2} \left(\frac{v}{c}\right)^{2/3} \qquad (8)$$

$$\frac{V_c}{V_p} = 30.25 \left(\frac{\rho_p}{\rho_T}\right)^{3/2} \left(\frac{v}{c}\right)^{2} \qquad (9)$$

It should be noted that these equations are based on the limited amount of data presently available and that the objective of this study was to develop equations suitable for engineering estimates of impact effects. Consequently, extrapolations to higher impact velocities are, as yet, largely unsupported by experimental data. However, micro-particle data[8] at an impact velocity of 10 km./sec. for steel projectiles impacting both copper and lead targets supports both the dependence of penetration on the two-thirds power of the impact velocity and the observation that high velocity impact craters (for particles larger than the material grain size) are hemispherical.

In order to illustrate the accuracy of Equations 8 and 9 and to compare them with Equations 1 and 2, the predicted values of $\left(P_c/D_s\right)$ and $\left(V_c/V_p\right)$, evaluated at $\left(v/c\right) = 1$, given by each expression have been plotted for each projectile-target system versus either K_1 or K_2. The results are shown in Figures 26 and 27. Dashed lines representing $\pm$ 10% error limits have been drawn on each curve. These curves illustrate the following:

1) that Equation 8 generally predicts depth of penetration more accurately than does Equation 1,

2) that the crater volume data are not accurately predicted by either of the equations, with Equation 9 possibly more accurate than Equation 2.

3) that the data in which aluminum alloys were used as targets are poorly predicted in all cases, and

4) that for systems in which the projectile and target materials were identical, both the penetration (K_1) and crater volume (K_2) data decrease in a manner that corresponds to increasing material strength or hardness properties.

The inability to predict cratering effects in the aluminum alloy targets could be due to a number of things. First, the data cover a range of impact velocities which does not extend to the value of the rod sound velocity (c) in these materials. Kineke[5] has established the following conditions for a truly hypervelocity impact:

1) the crater must be hemispherical in shape, and

2) the component of the impact velocity normal to the target surface must be greater than the velocity of a plastic (dilatational)wave in the target.

The dilatational wave velocity for the aluminum alloys (approximately 6.2 km./sec.) exceeds the rod sound velocity - consequently, even though these data fall within the $\left(P_c/D_c\right)$ limits established for this investigation the maximum impact velocity falls far short of the dilatational velocity. Second, the properties (shear strength, hardness, etc.) of aluminum alloys vary over a wide range. While no strong effect at high velocities due to material strength or hardness

has been indicated by the remainder of the data, the aluminum alloy target data combine a relatively low maximum test velocity (when compared with the dilatational wave velocity) with relatively high strength target materials, possibly resulting in a strong low velocity-material strength effect. Additional, higher velocity data for these alloys are required to clarify this issue.

The variation in K_1 and K_2 for the identical projectile-target material systems indicate that penetration and crater volume are also dependent upon a weak function of the target material properties. Several authors have suggested, based upon either experimental results or theoretical considerations, that impact cratering is dependent upon various mechanical or physical properties of the target material. Rinehart and Pearson[9], and Palmer[10], et. al., have found that target shear strength is an important parameter. Allison[11], Summers[1], and Feldman[12] have shown effects due to variations in target Brinell hardness. Within the limitations of the present study, however, these parameters do not appear to have a strong effect. As in the case of the aluminum alloy data, additional higher velocity data are needed before a definite conclusion can be reached.

IMPACT AT OBLIQUE INCIDENCE

The preceeding section was limited to an analysis of the case in which the projectile approaches the target along the normal to the target surface. This section is devoted to an examination of the data which apply to the related problem of impact at angles of incidence other than normal.

Crater Profile

The limited amount of data illustrating the variation of $\left(P_c/D_c\right)$ with impact velocity at oblique angles of incidence are presented in Figure 28. The crater profiles produced when steel projectiles impact against lead targets at both normal and oblique angles of incidence are compared at equal values of normal impact velocity. The oblique impact data represent a series of tests at 60° incidence in which both the mass and total velocity of the projectile were varied and a series of tests in which angle of incidence was varied while projectile mass and total velocity were held constant. It is apparent from these data that the characteristic high velocity crater shape is realized in oblique impact at roughly the same value of normal impact velocity as is required in normal impact. It is also evident that the low velocity peak in $\left(P_c/D_c\right)$ observed under normal impact is not present for low values of normal velocity under oblique impact conditions. In oblique impact, low normal velocities are associated either with very high total velocity - high angle of obliquity impact or with low total velocity - low angle of obliquity impact.

Further evidence that the characteristic high velocity crater shape is reached in oblique impact at high values of normal impact velocity is presented in Figure 29. A comparison of the ratio of the diameter of the crater mouth that is in line with the projectile trajectory ($D_{C\ MAJ}$) to the diameter at right angles to the projectile trajectory ($D_{C\ MIN}$), both measured in the plane of the undamaged target

surface, indicates that the craters produced are circular at high values of normal impact velocity.

Depth of Penetration

Data illustrating the variation of the penetration parameter, (P_c/D_s), with the impact velocity parameter, (v/c), for oblique angles of incidence are presented in Figures 30 and 31. Here data obtained by impacting copper spheres with copper targets and by impacting steel into lead at both normal and oblique angles of incidence are compared at equal values of normal impact velocity. The data indicate that under high velocity conditions, projectiles of equal mass impacting at either normal or oblique incidence penetrate to the same depth provided they have the same velocity normal to the surface. In the case of steel impacting into lead at oblique incidence, the typical transition region between undeformed projectile penetration and high velocity penetration is not present. This supports the earlier observation that the low velocity (P_c/D_c) overshoot does not occur in oblique impact.

The combined crater profile and penetration data indicate that, under high velocity impact conditions, it is impossible to determine either causitive particle mass or velocity by examination of a crater. Consequently, to the extent that the surface of the Earth and Moon react as ductile metals under high velocity impact conditions, these data invalidate calculations of the mass and velocity of the meteorites responsible for terrestrial or lunar craters that are based only on observations of the craters.

CONCLUSIONS

A thorough review has been made of existing experimental data applicable to the impact of individual high velocity metal projectiles with semi-infinite metal targets. The following empirical relations,

$$\frac{P_c}{D_s} = 1.96\left(\frac{\rho_p}{\rho_t}\right)^{1/2}\left(\frac{v}{c}\right)^{2/3}$$

and

$$\frac{V_c}{V_p} = 30.25\left(\frac{\rho_p}{\rho_t}\right)^{3/2}\left(\frac{v}{c}\right)^{2}$$

relating depth of penetration and crater volume to properties of the projectile and target have been derived based upon the following assumptions.

1) projectile shape and orientation do not affect crater size or shape, and

2) high velocity craters are hemispherical in shape.

Both of these assumptions are supported by experimental results; however, the first must be qualified slightly to apply only to either spherical projectiles or to cylindrical projectiles up to one caliber in length.

It should be noted that the objective of this study was to determine whether an analysis of the total body of impact data would result in a compatible set of equations of sufficient accuracy for engineering design purposes. The extension of the results to conditions not covered by the available data involves certain elements of uncertainty; however, some evidence is available which indicates that the trends established by these data appear at velocities of 10km./sec.

Evidence has also been presented which indicates that, under high velocity conditions, particles of equal mass impacting at either normal or oblique incidence produce identical craters providing they have the same velocity normal to the surface.

REFERENCES

1. Summers, J. L., October, 1959, Investigation of high speed impact regions of impact and impact at oblique angles: NASA, TN D-94.

2. Huth, J. H., Thompson, J. S., and Van Valkenburg, M. E., 1957, Some new data on high speed impact phenomena: Jour. Appl. Mech., v. 24, March, p. 65.

3. Charters, A. C. and Locke, G. S. Jr., May 28, 1958, A preliminary investigation of high speed impact: the penetration of small spheres into thick copper targets: NASA, RM A58B26.

4. Kineke, J. H., Jr., 1959, An experimental study of crater formation in lead: Proceedings of the Third Symposium on Hypervelocity Impact, v. 1, February, p. 157.

5. Kineke, J. H., Jr., 1960, An experimental study of crater formation in metallic targets: Hypervelocity Impact - Fourth Symposium, v. 1, September, p. 10.

6. Atkins, W. W., 1960, Hypervelocity penetration study: Hypervelocity Impact - Fourth Symposium, v. 1, September, p. 11.

7. Maiden, C. J., Tardif, H. P., and Charest, J., 1960, An investigation of spalling and crater formation by hypervelocity particles: Hypervelocity Impact - Fourth Symposium, v. III, September, p. 38.

8. Gehring, J. H., Jr., and Richards, L. G., 1960, Further studies of microparticle cratering in a variety of target materials: Hypervelocity Impact - Fourth Symposium, v. III, September, p. 34.

9. Rinehart, J. S. and Pearson, J., 1954, Behavior of metals under impulsive loads Cleveland, Ohio, American Society for Metals.

10. Palmer, E. P., Grow, R. W., Johnson, D. K., and Turner, G. H., 1960, Cratering; experiment and theory: Hypervelocity Impact - Fourth Symposium, v. I, September, p. 13.

11. Allison, F. E., 1959, A review of the theories concerning crater formation by hypervelocity impact: Proceedings of the Third Symposium on Hypervelocity Impact, v. 1, February, p. 287.

12. Feldman, J. B., Jr., 1960, Volume - energy relation from shaped charge jet penetrations: Hypervelocity Impact - Fourth Symposium, v. II, September, p. 26.

13. Collins, R. D., Jr. and Kinard, W. H., May, 1960, The dependency of penetration on the momentum per unit area of the impacting projectile and the resistance of materials to penetration: NASA, TN D-238.

14. Van Fleet, H. B., Whited, C. R., and Partridge, W. S., January, 1958, High velocity impact craters in lead-tin alloys: University of Utah, Technical Report No. OSR-13.

15. Ferguson, W. J. and Mc Kinney, K. R., November 19, 1959, The influence of temperature elevation on the penetration of missiles into copper targets: NRL Report, 5407.

16. Culp, F. L., 1959, Volume - energy relation for craters formed by high velocity projectiles: Proceedings of the Third Symposium on Hypervelocity Impact, v. 1, February, p. 141.

17. Partridge, W. S., 1957, High velocity impact studies at the University of Utah Proceedings of the Second Hypervelocity and Impact Effects Symposium, v. 1, December, p. 93.

BLANK PAGE

VARIATION OF CRATER PROFILE PARAMETER WITH IMPACT VELOCITY FOR VARIOUS PROJECTILE MATERIALS AND ALUMINUM TARGETS

FIGURE - 1

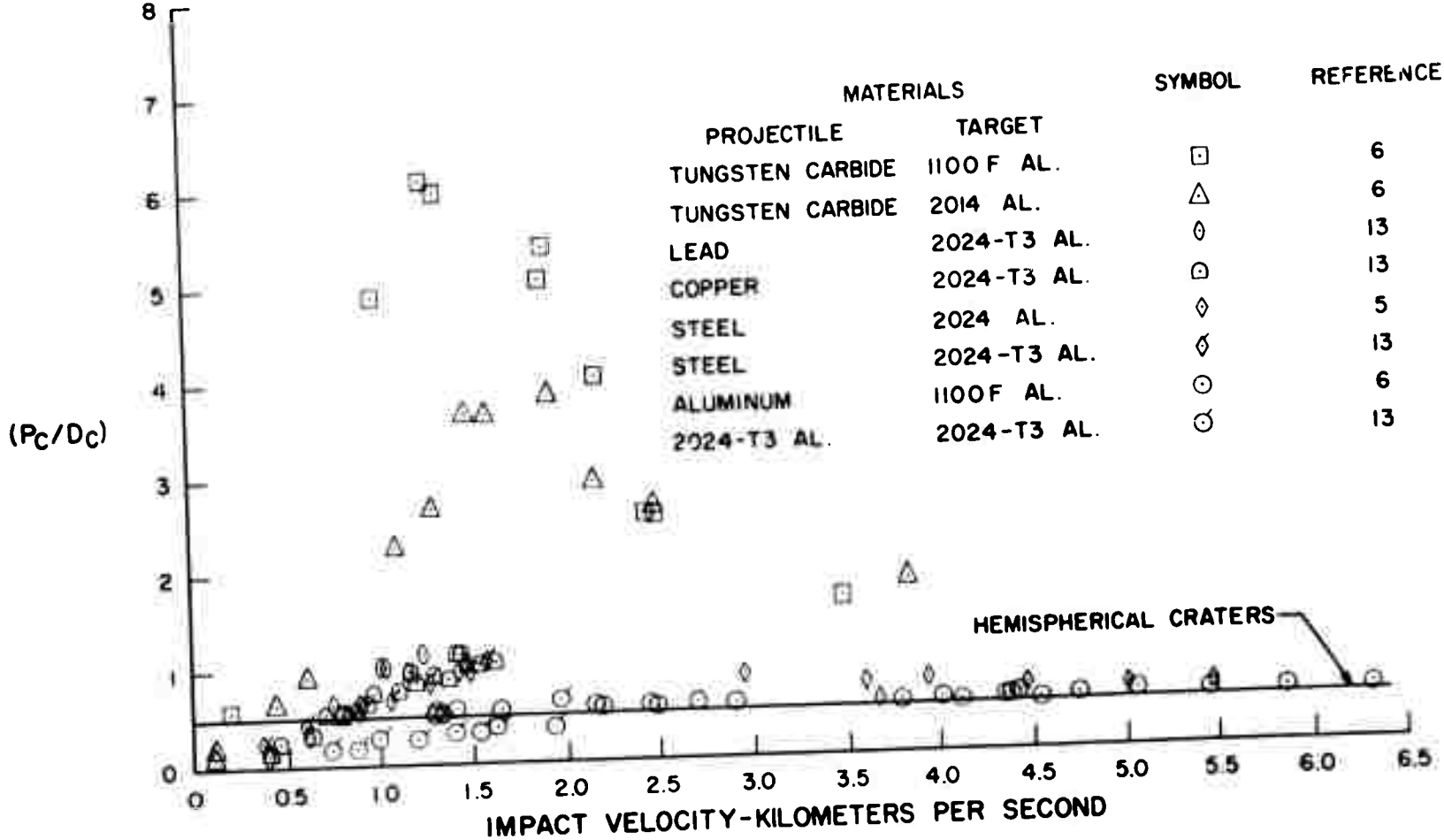

VARIATION OF CRATER PROFILE PARAMETER WITH IMPACT VELOCITY FOR STEEL PROJECTILES AND ZINC TARGETS

FIGURE-2

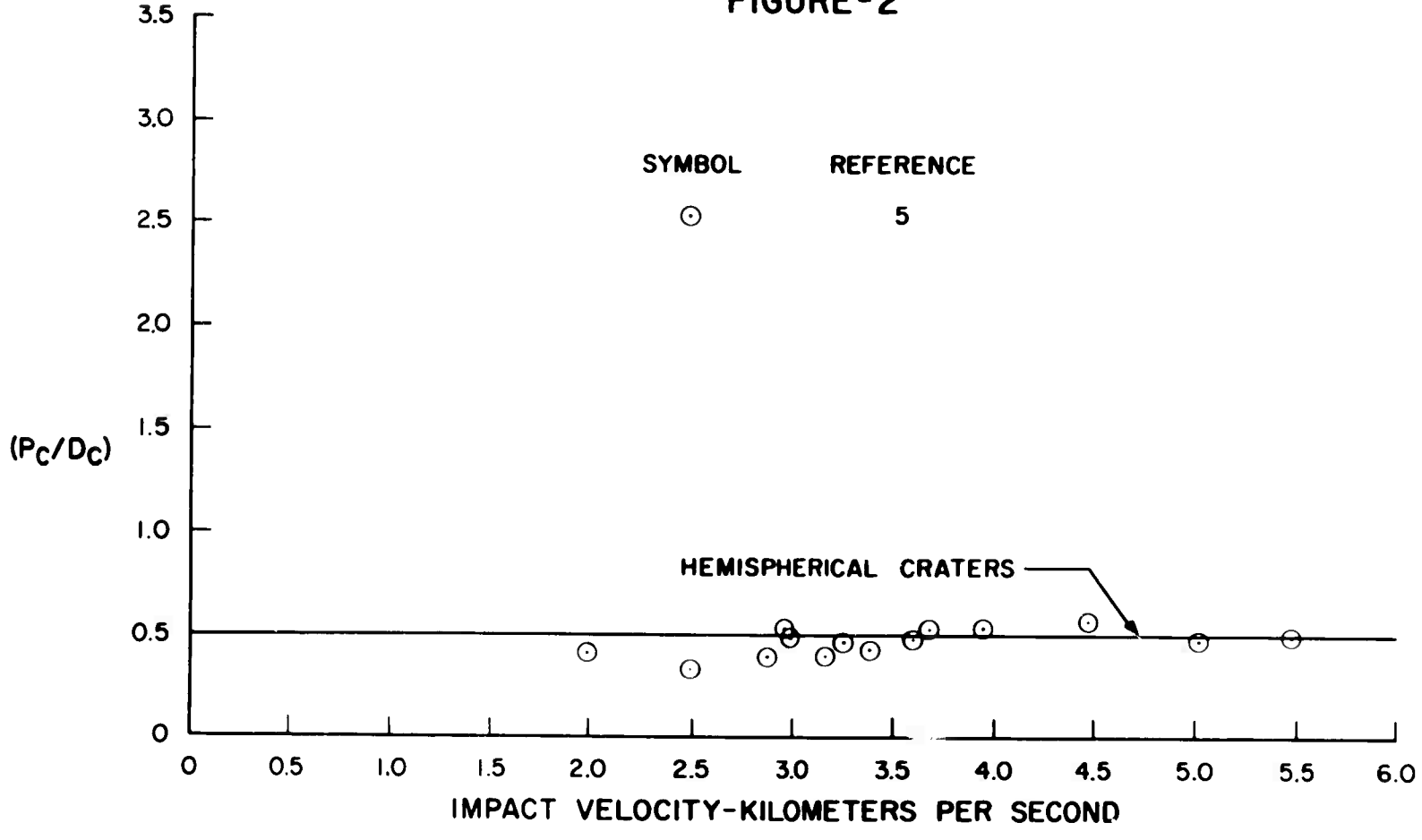

VARIATION OF CRATER PROFILE PARAMETER WITH IMPACT VELOCITY FOR TIN PROJECTILES AND TIN TARGETS

FIGURE-3

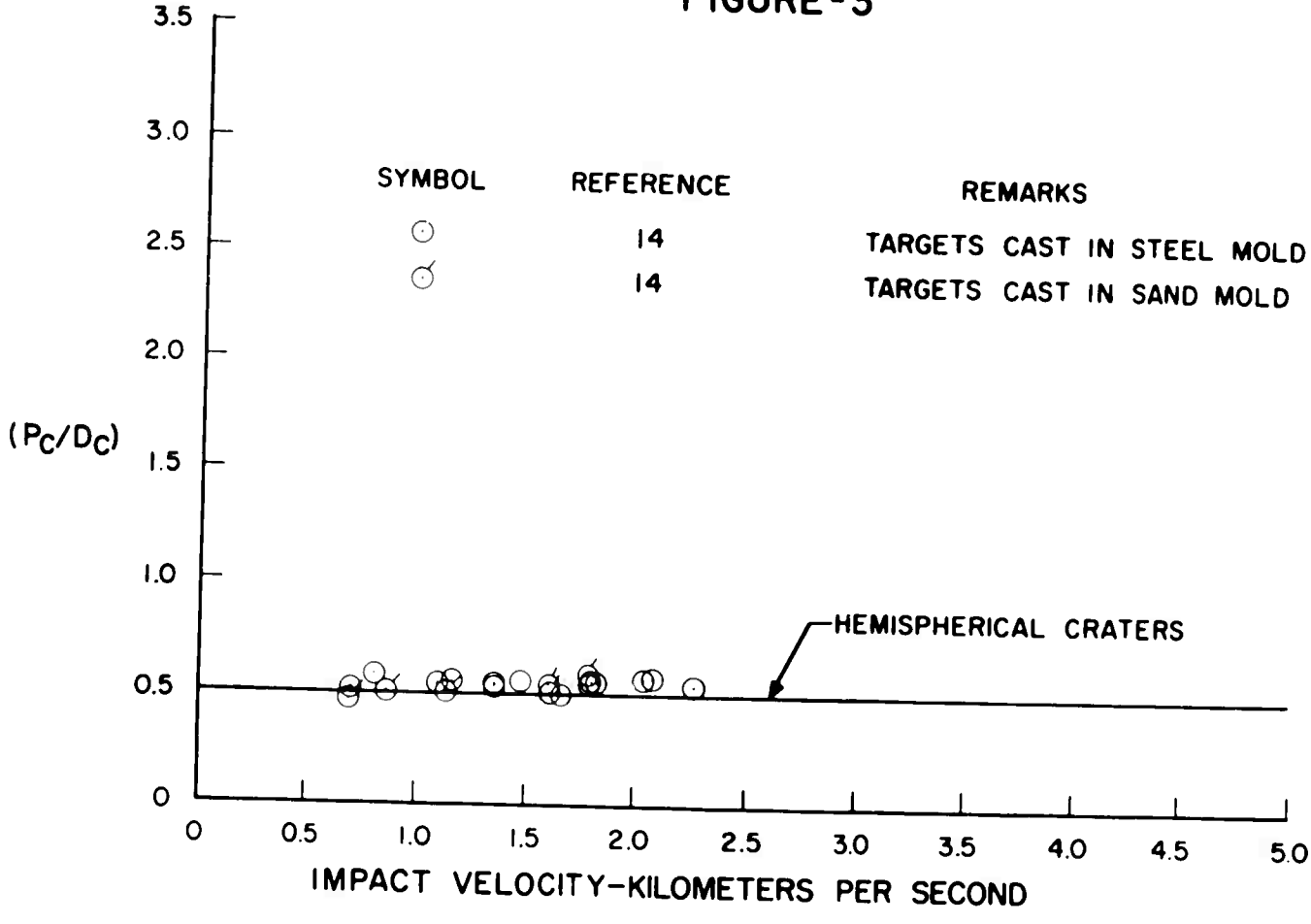

VARIATION OF CRATER PROFILE PARAMETER WITH IMPACT VELOCITY FOR VARIOUS PROJECTILE MATERIALS AND STEEL TARGETS

FIGURE - 4

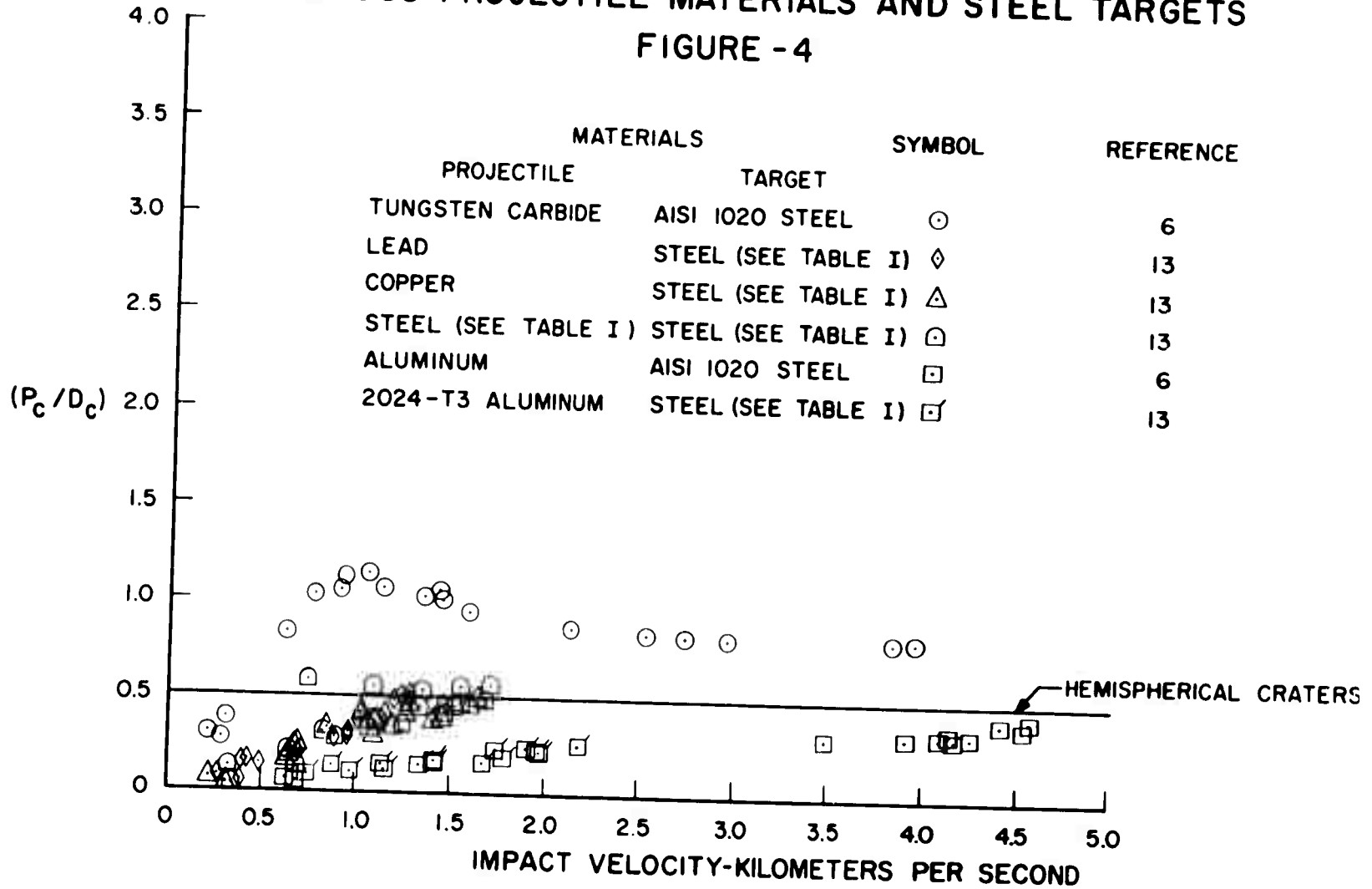

VARIATION OF CRATER PROFILE PARAMETER WITH IMPACT VELOCITY FOR STEEL PROJECTILES AND CADMIUM TARGETS

FIGURE - 5

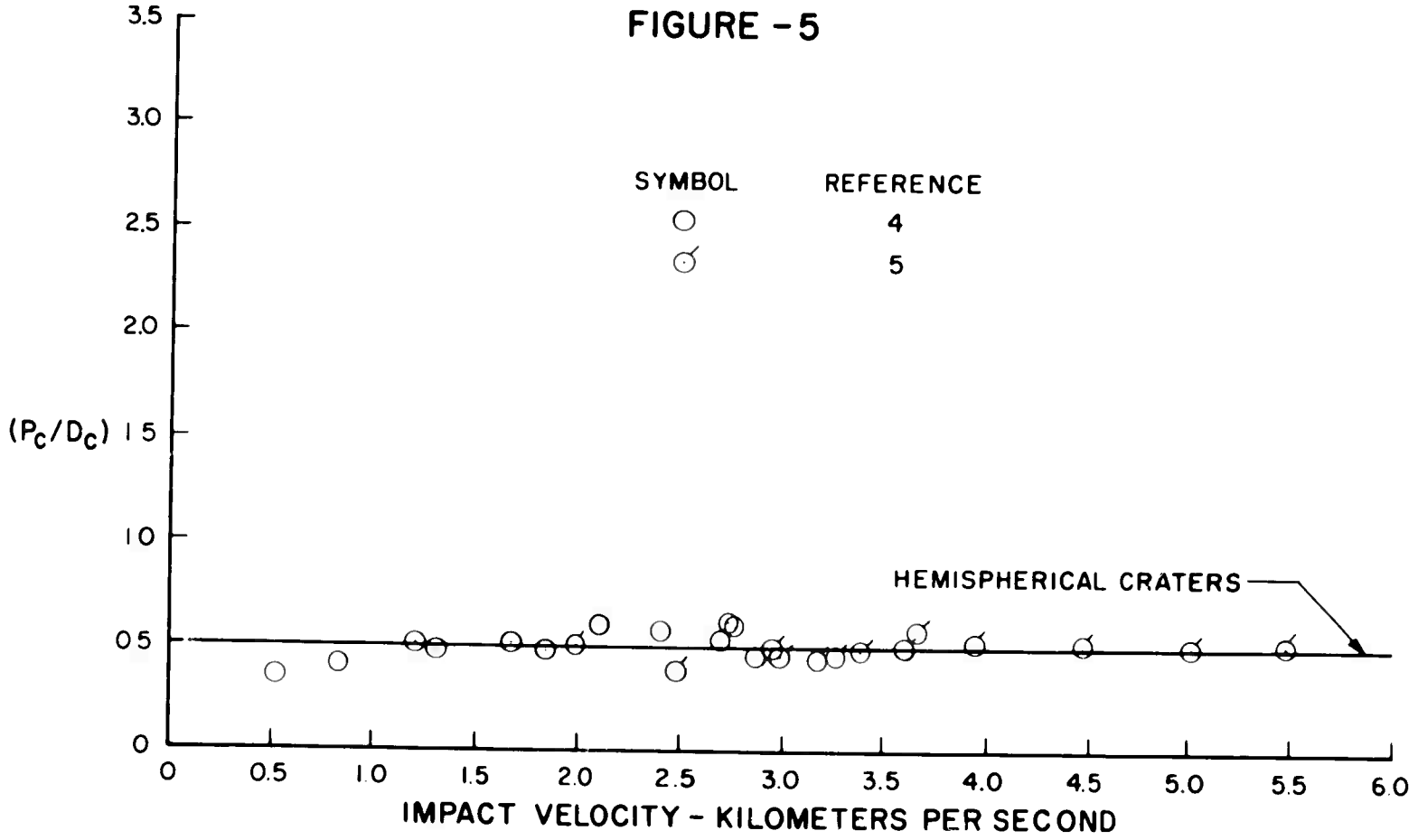

VARIATION OF CRATER PROFILE PARAMETER WITH IMPACT VELOCITY FOR VARIOUS PROJECTILE MATERIALS AND COPPER TARGETS

FIGURE - 6

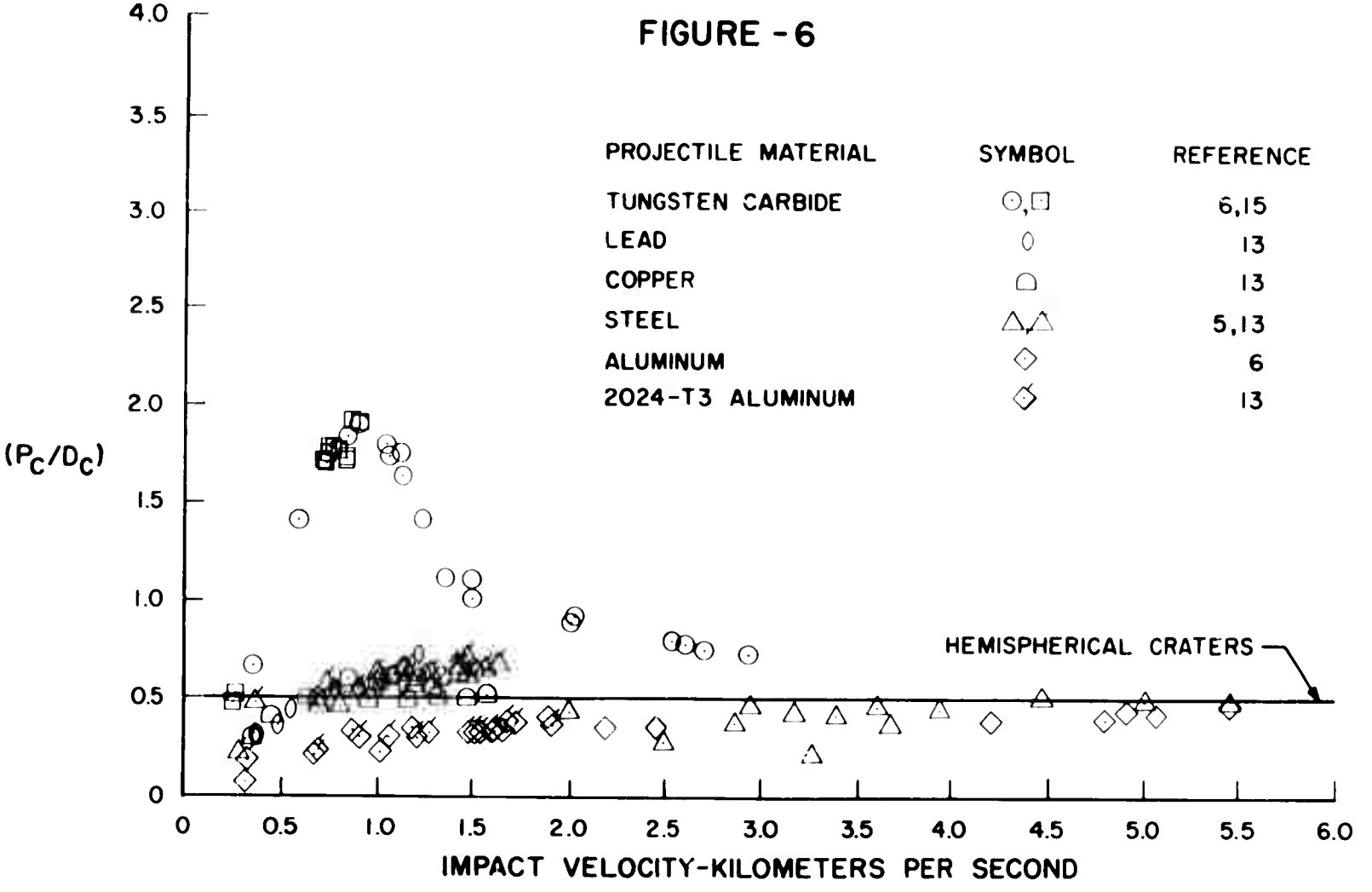

VARIATION OF CRATER PROFILE PARAMETER WITH IMPACT VELOCITY FOR VARIOUS PROJECTILE MATERIALS AND LEAD TARGETS

FIGURE-7

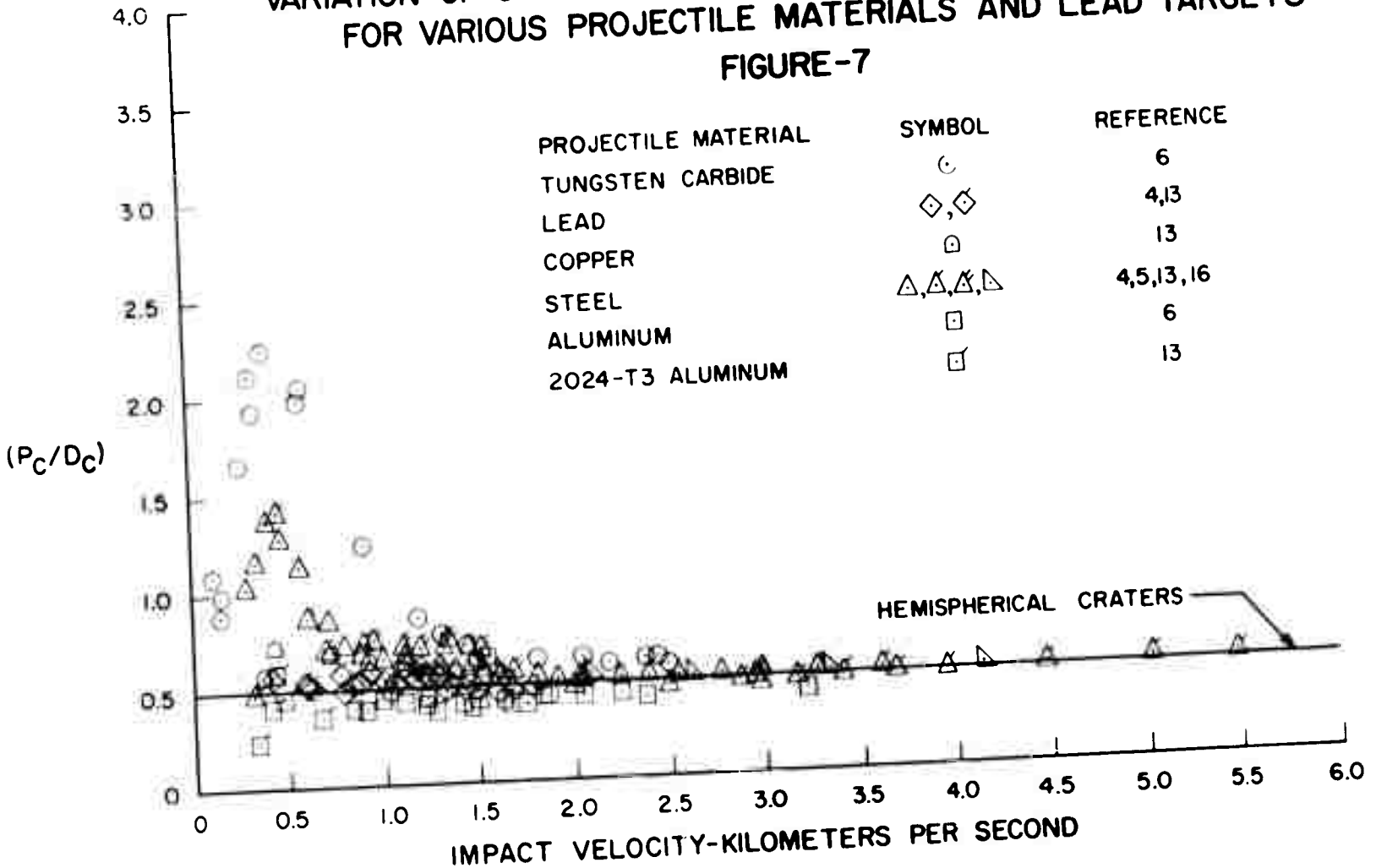

VARIATION OF PENETRATION PARAMETER WITH IMPACT VELOCITY PARAMETER FOR ALUMINUM PROJECTILES AND ALUMINUM ALLOY TARGETS

FIGURE-8a

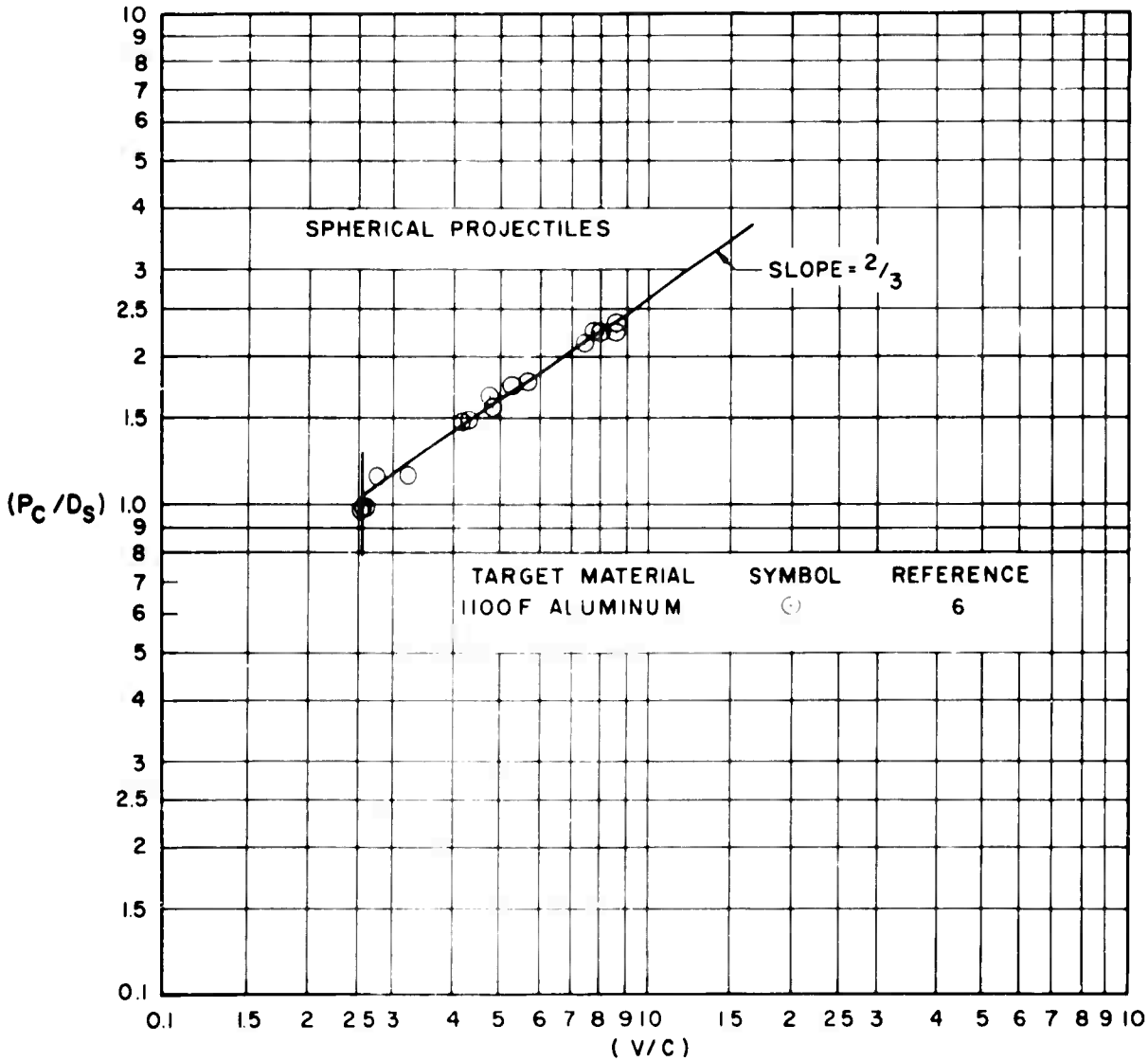

VARIATION OF PENETRATION PARAMETER WITH IMPACT VELOCITY PARAMETER FOR ALUMINUM ALLOY PROJECTILES AND TARGETS

FIGURE-8b

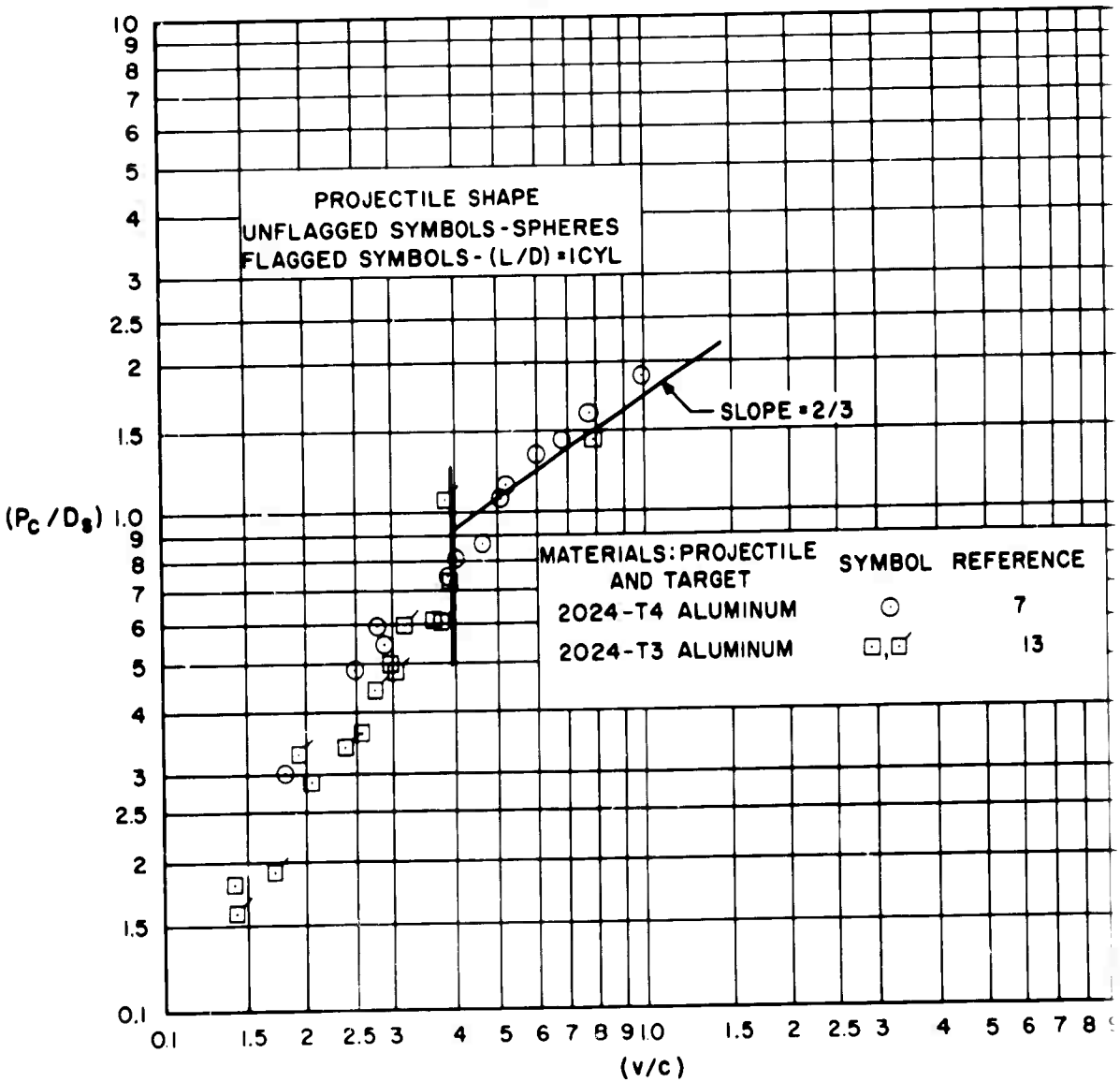

VARIATION OF PENETRATION PARAMETER WITH IMPACT VELOCITY PARAMETER FOR ZINC PROJECTILES AND TARGETS

FIGURE – 9a

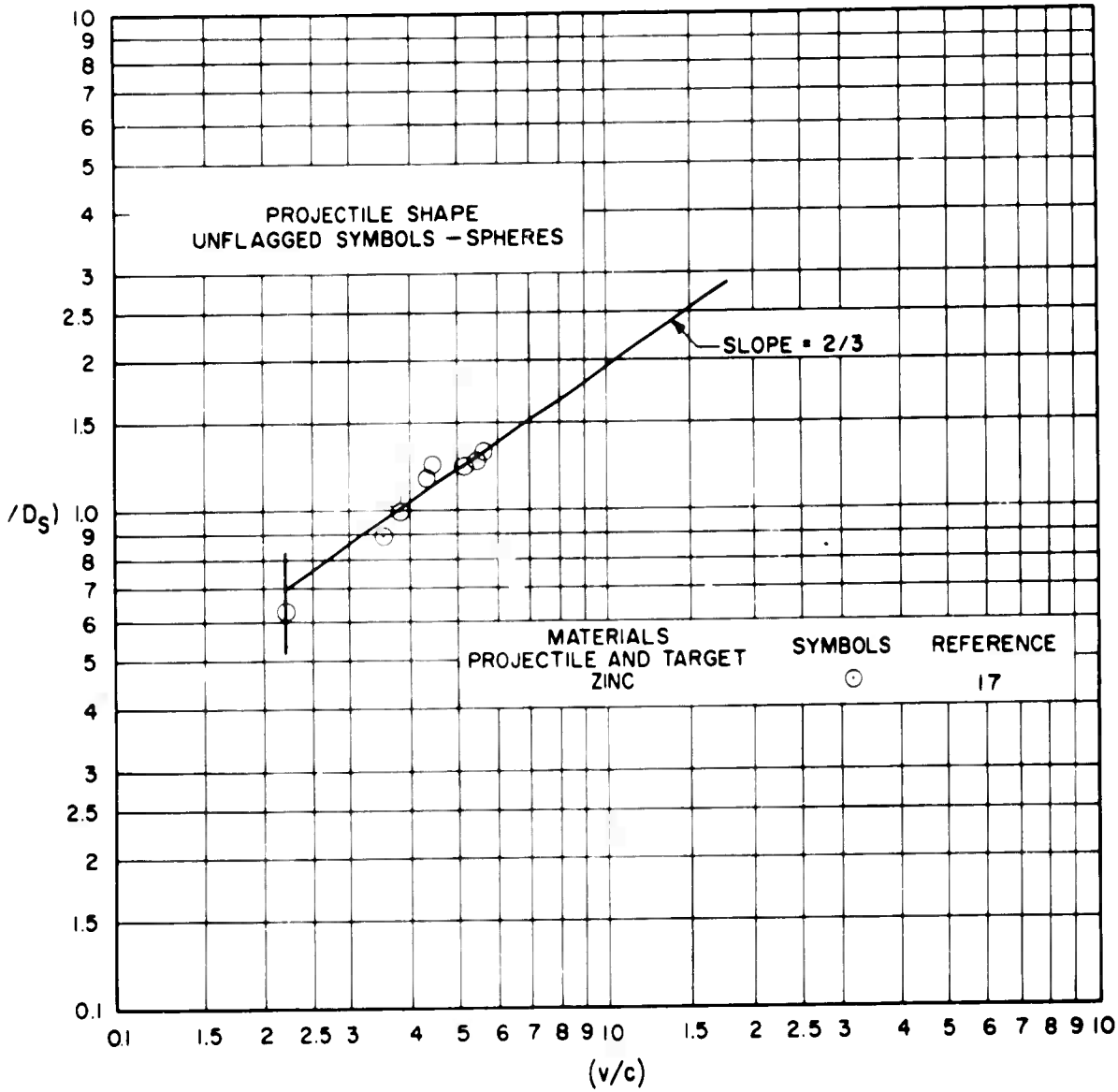

VARIATION OF PENETRATION PARAMETER WITH IMPACT VELOCITY PARAMETER FOR STEEL PROJECTILES AND ZINC TARGETS

FIGURE-9b

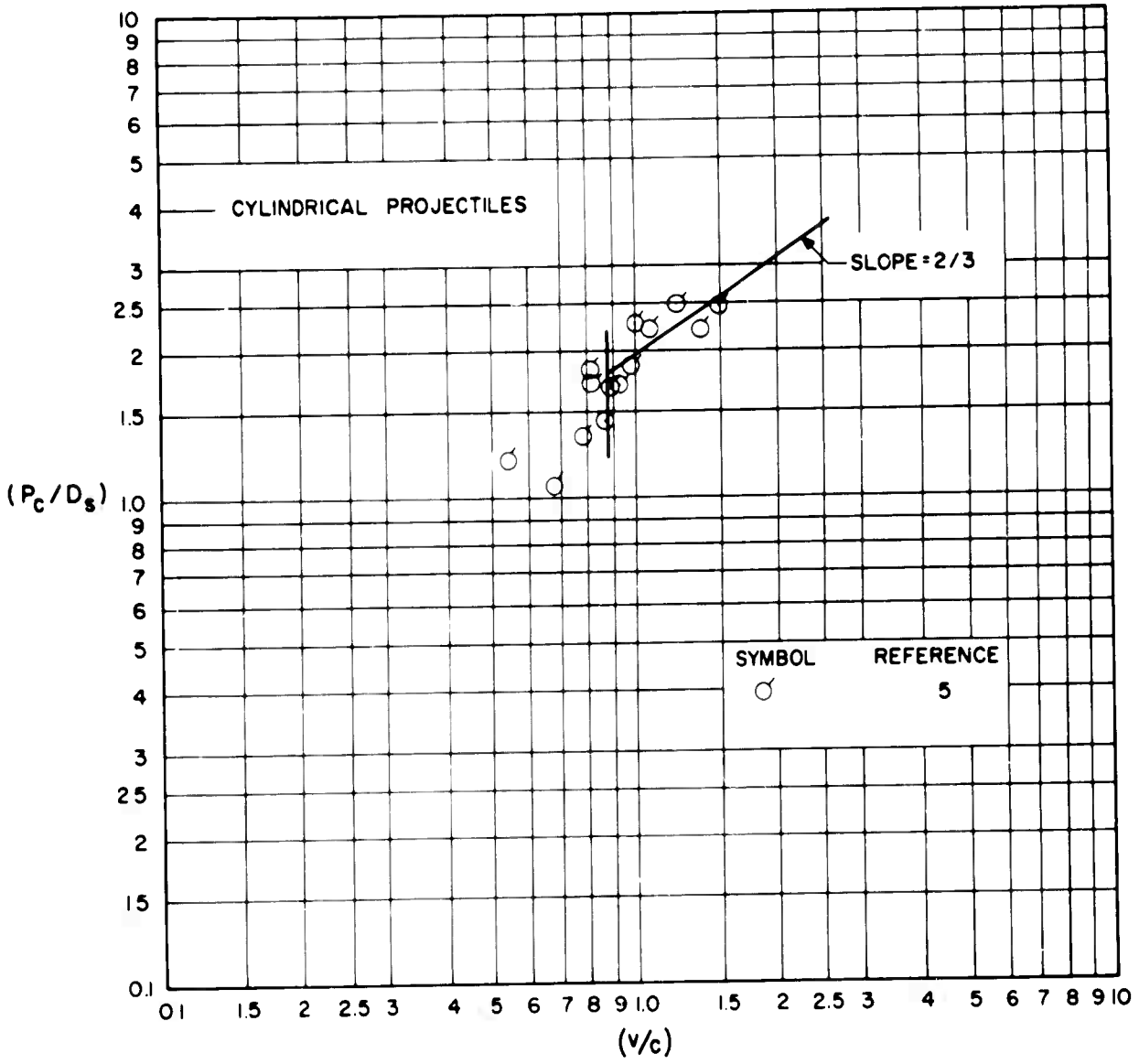

VARIATION OF PENETRATION PARAMETER WITH IMPACT VELOCITY PARAMETER FOR TIN PROJECTILES AND TARGETS

FIGURE-10

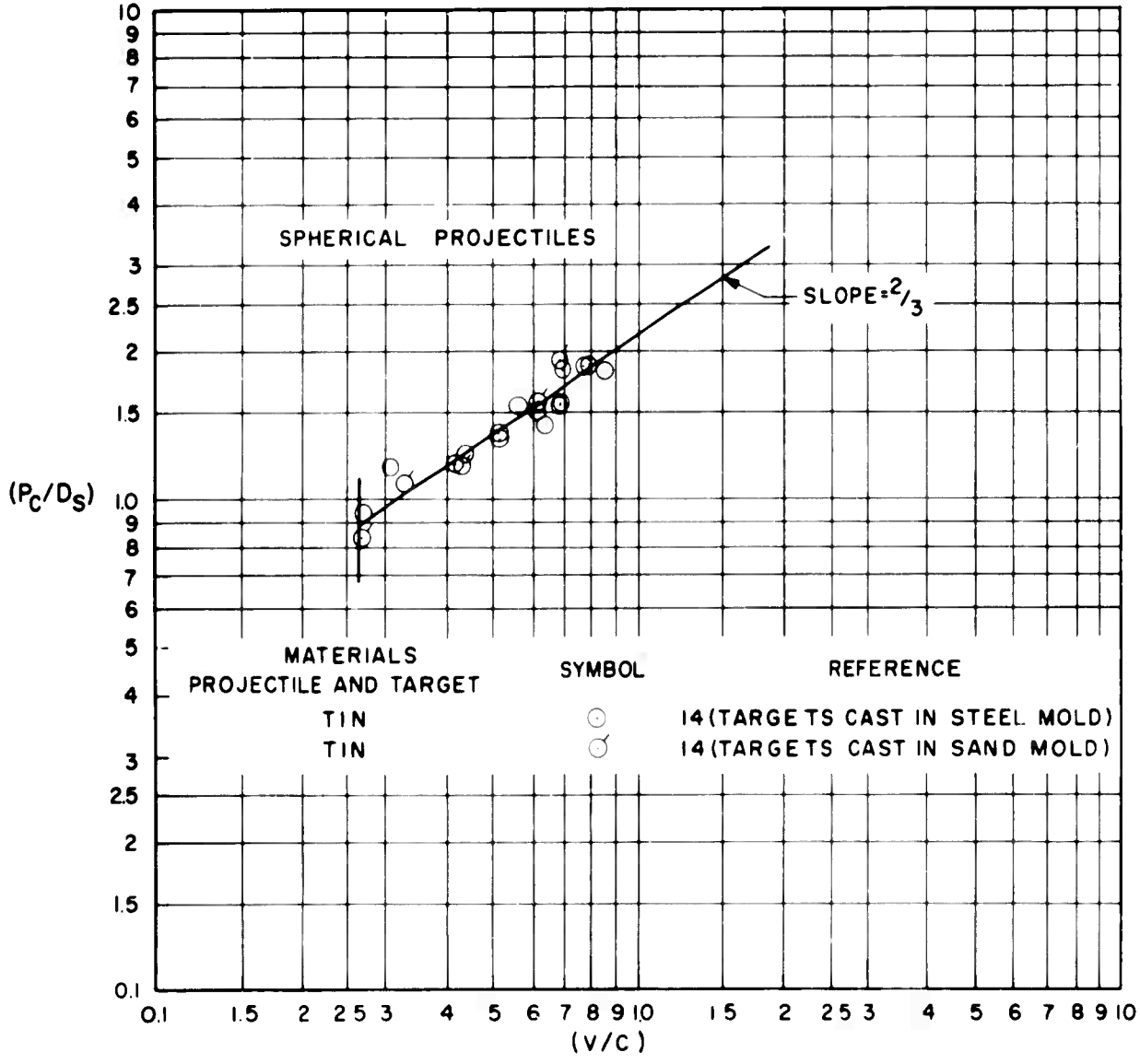

VARIATION OF PENETRATION PARAMETER WITH IMPACT VELOCITY PARAMETER FOR STEEL PROJECTILES AND TARGETS

FIGURE-11

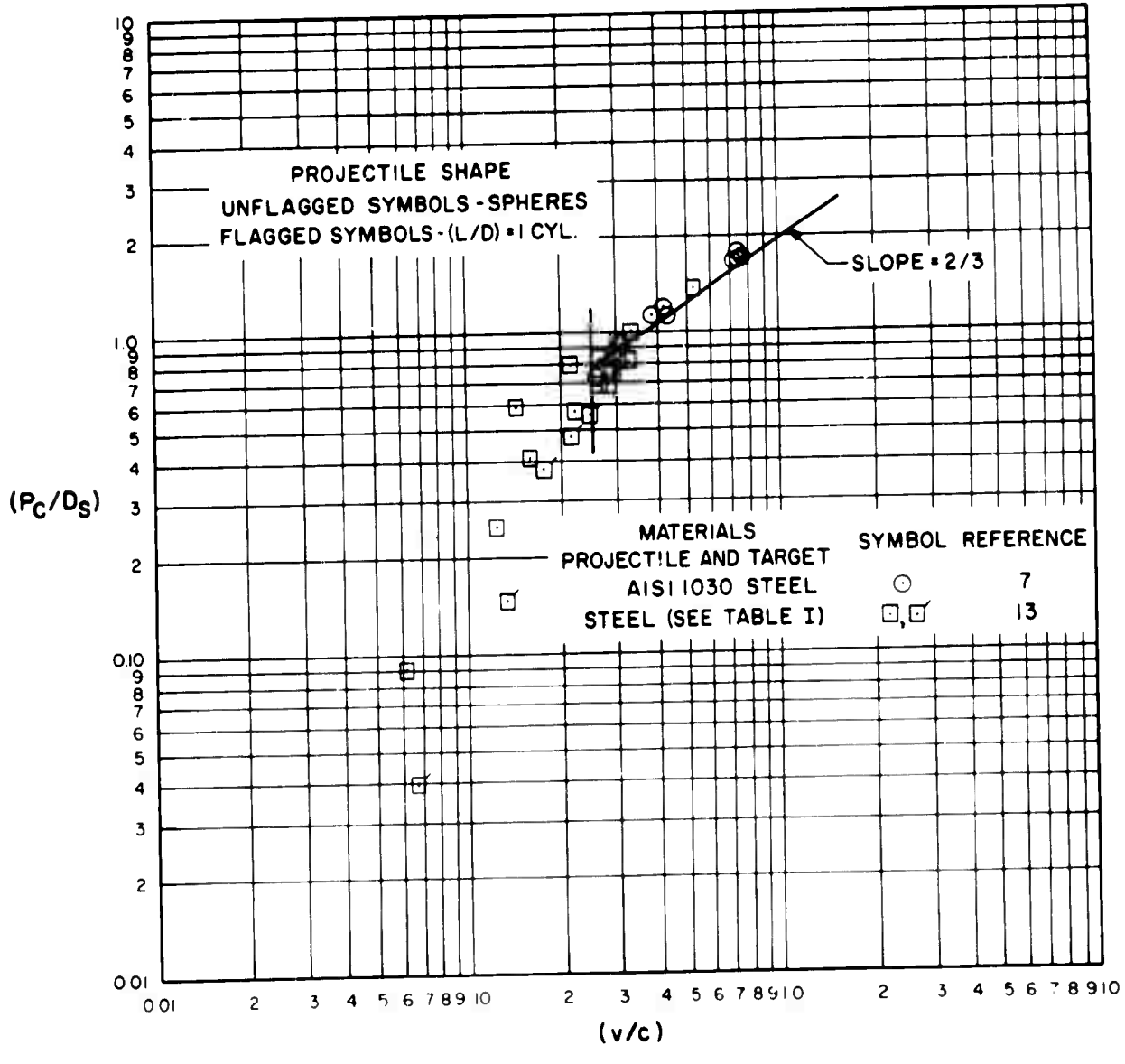

VARIATION OF PENETRATION PARAMETER WITH IMPACT VELOCITY PARAMETER FOR STEEL PROJECTILES AND CADMIUM TARGETS

FIGURE-12

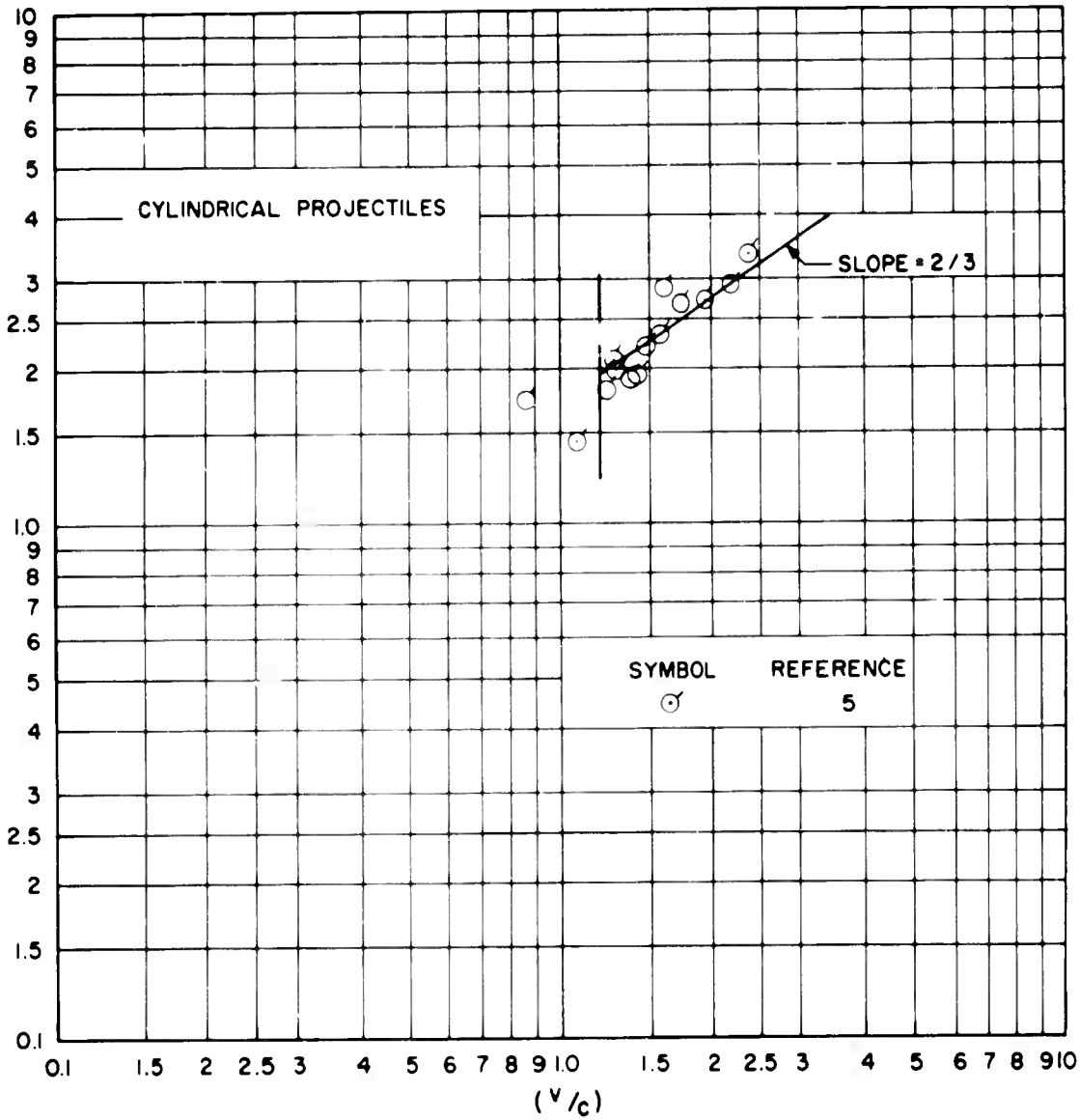

VARIATION OF PENETRATION PARAMETER WITH IMPACT VELOCITY PARAMETER FOR ALUMINUM ALLOY PROJECTILES AND COPPER TARGETS

FIGURE-13a

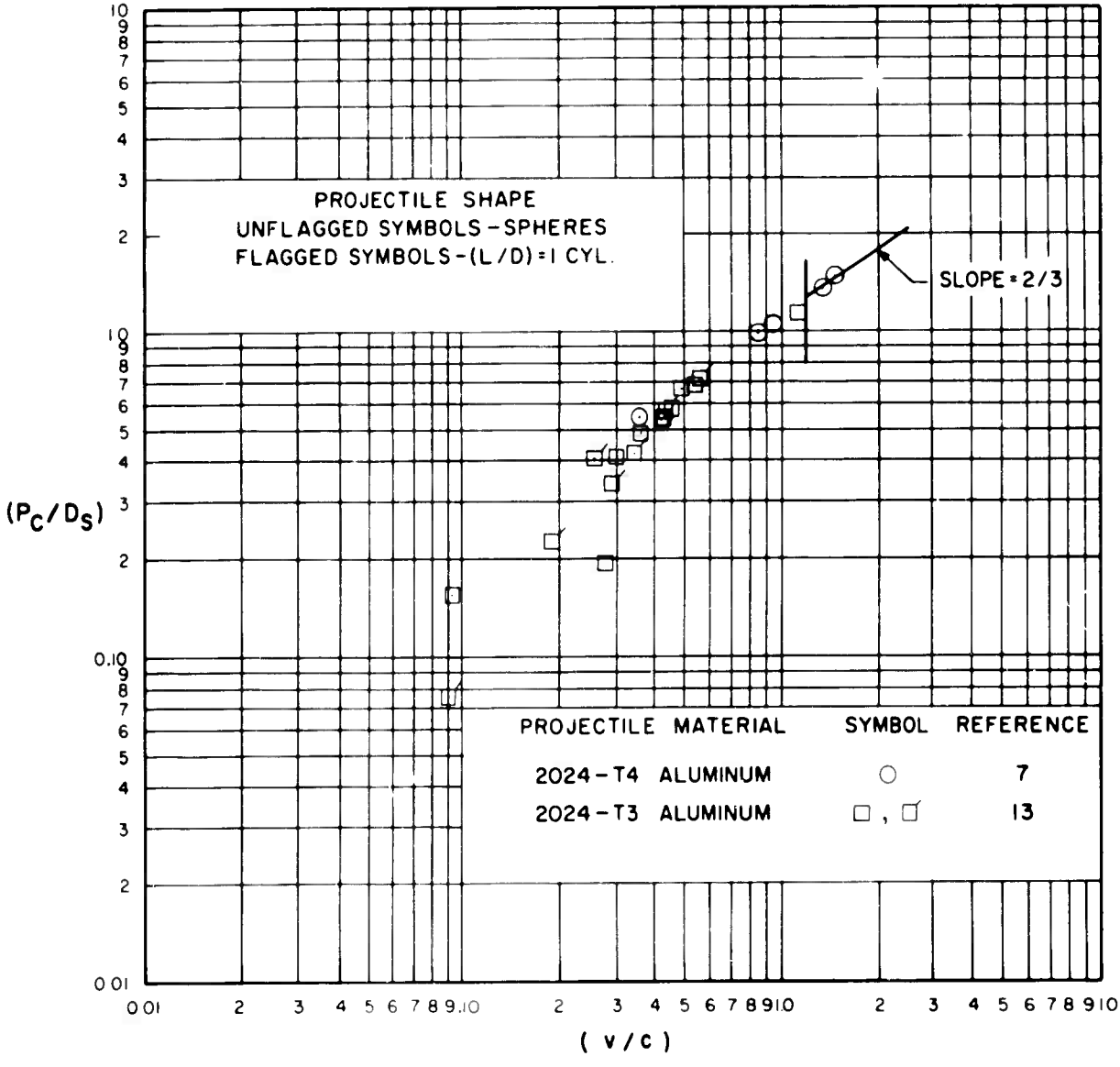

VARIATION OF PENETRATION PARAMETER WITH IMPACT VELOCITY PARAMETER FOR STEEL PROJECTILES AND COPPER TARGETS

FIGURE-13b

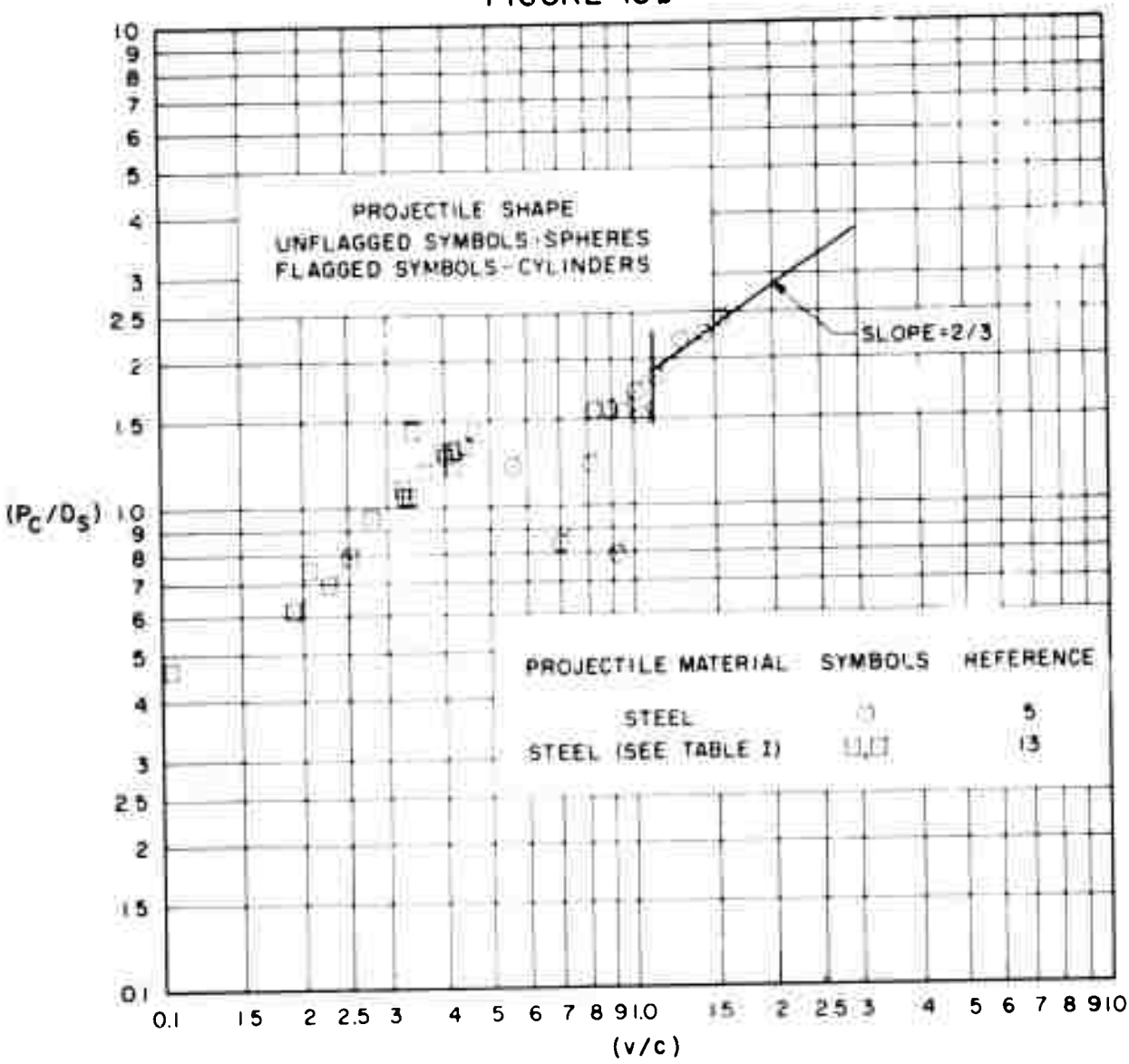

VARIATION OF PENETRATION PARAMETER WITH IMPACT VELOCITY PARAMETER FOR COPPER PROJECTILES AND TARGETS

FIGURE-13c

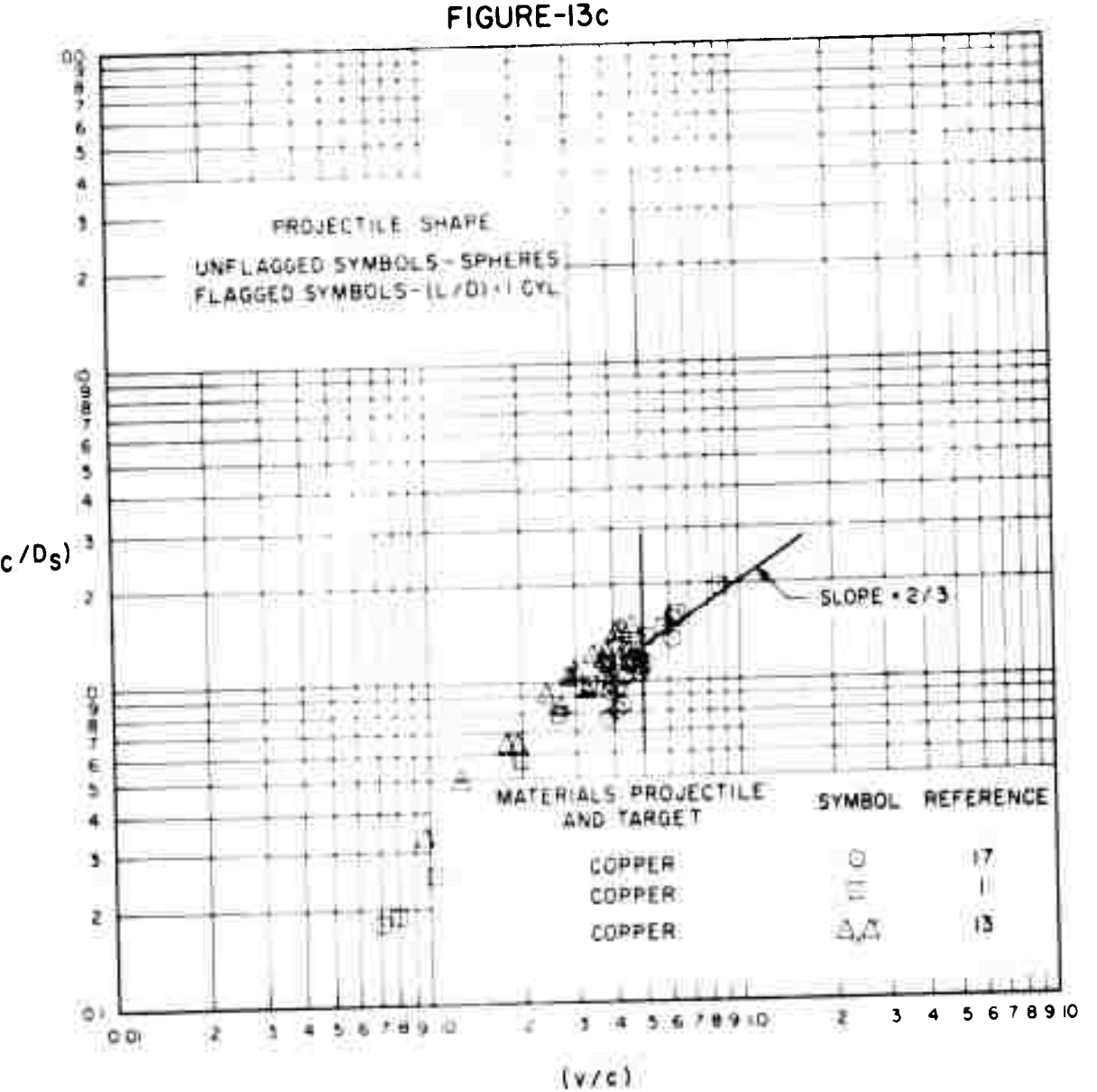

VARIATION OF PENETRATION PARAMETER WITH IMPACT VELOCITY PARAMETER FOR ALUMINUM ALLOY PROJECTILES AND LEAD TARGETS

FIGURE-14a

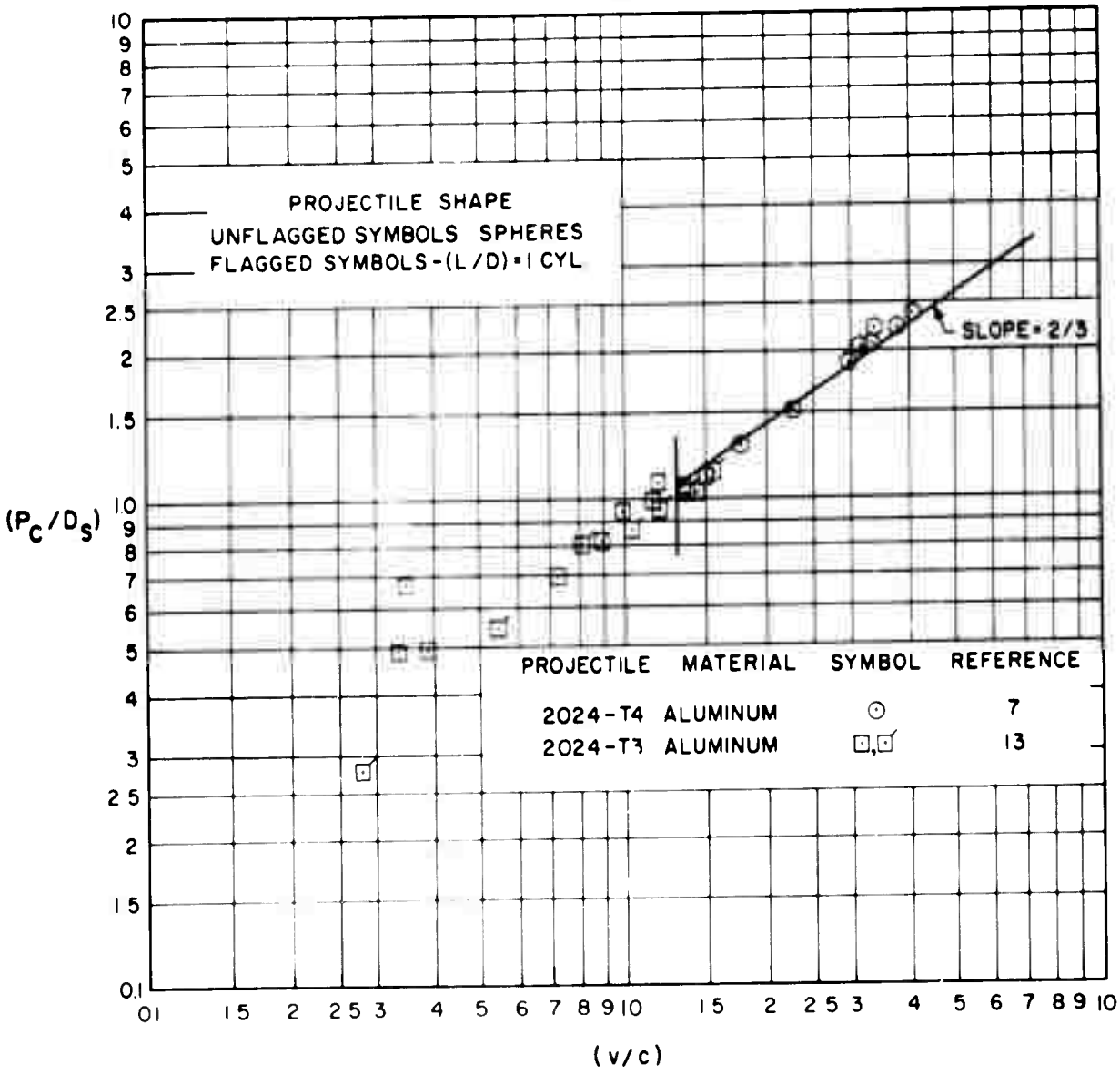

VARIATION OF PENETRATION PARAMETER WITH IMPACT VELOCITY PARAMETER FOR STEEL PROJECTILES AND LEAD TARGETS

FIGURE-14b

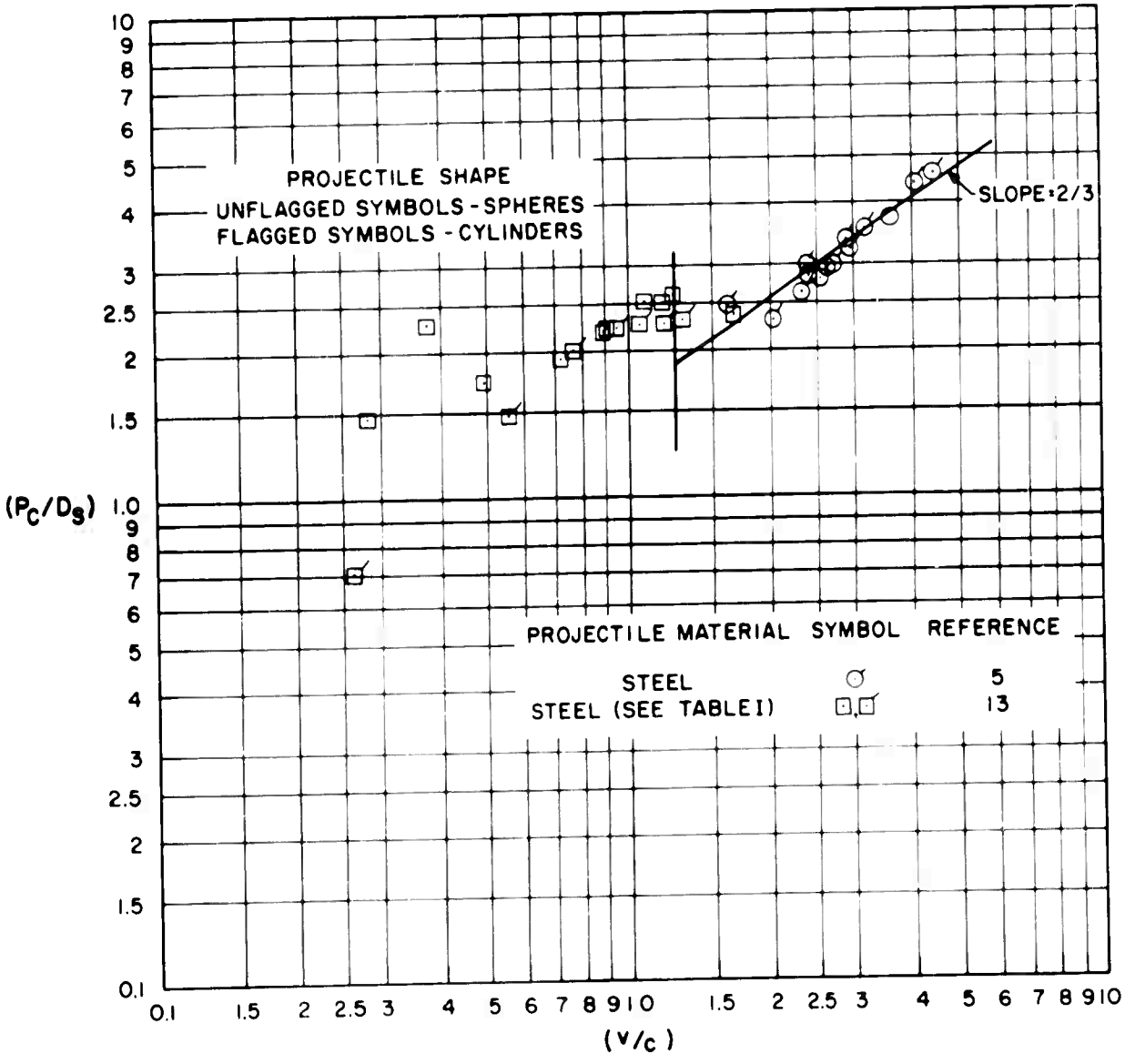

VARIATION OF PENETRATION PARAMETER WITH IMPACT VELOCITY PARAMETER FOR COPPER PROJECTILES AND LEAD TARGETS

FIGURE-14c

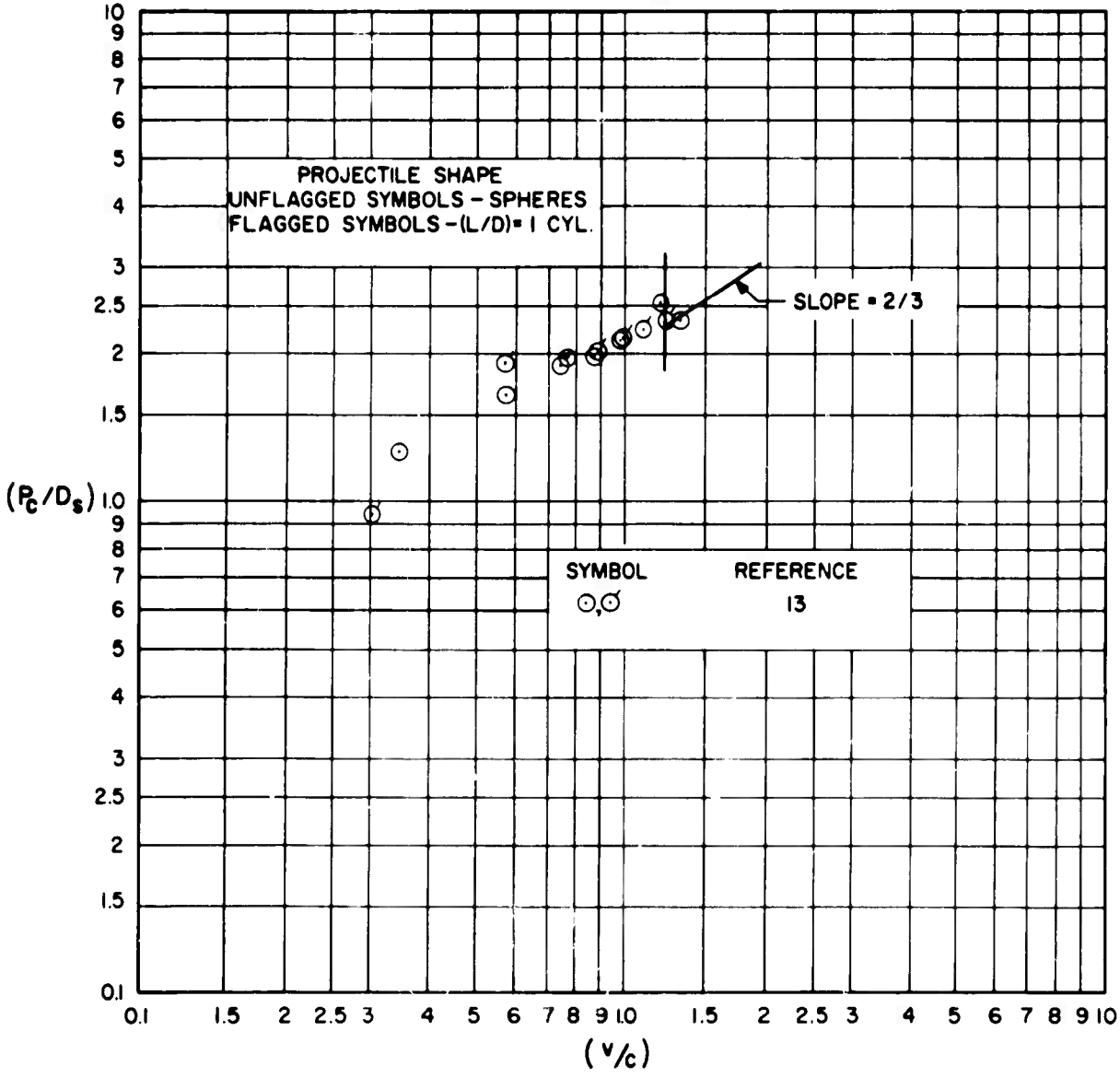

VARIATION OF PENETRATION PARAMETER WITH IMPACT VELOCITY PARAMETER FOR LEAD PROJECTILES AND TARGETS

FIGURE-14d

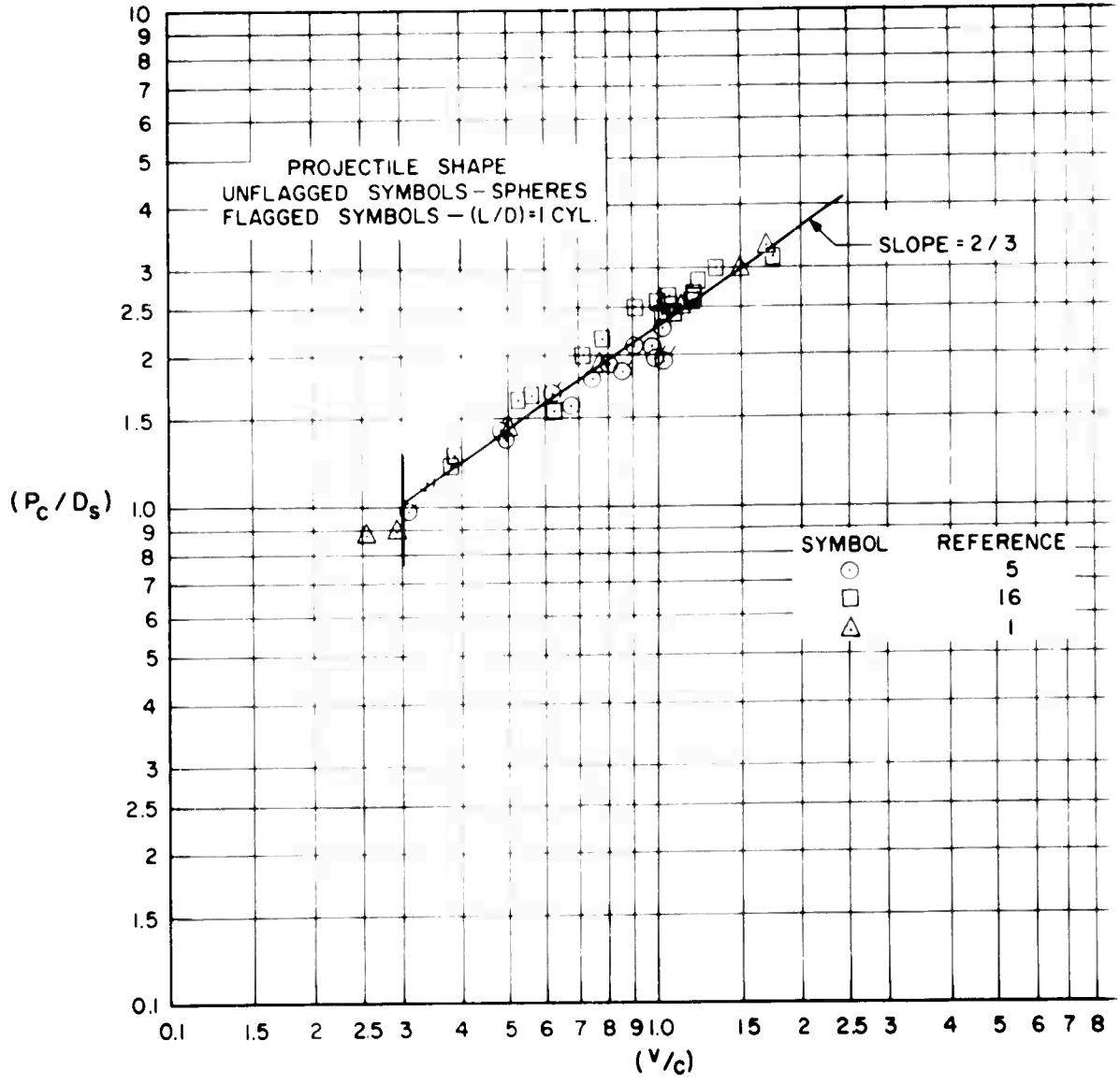

ATION OF CRATER VOLUME PARAMETER WITH IMPACT VELOCITY PARAMETER FOR ALUMINUM PROJECTILES AND ALUMINUM ALLOY TARGETS

FIGURE-15a

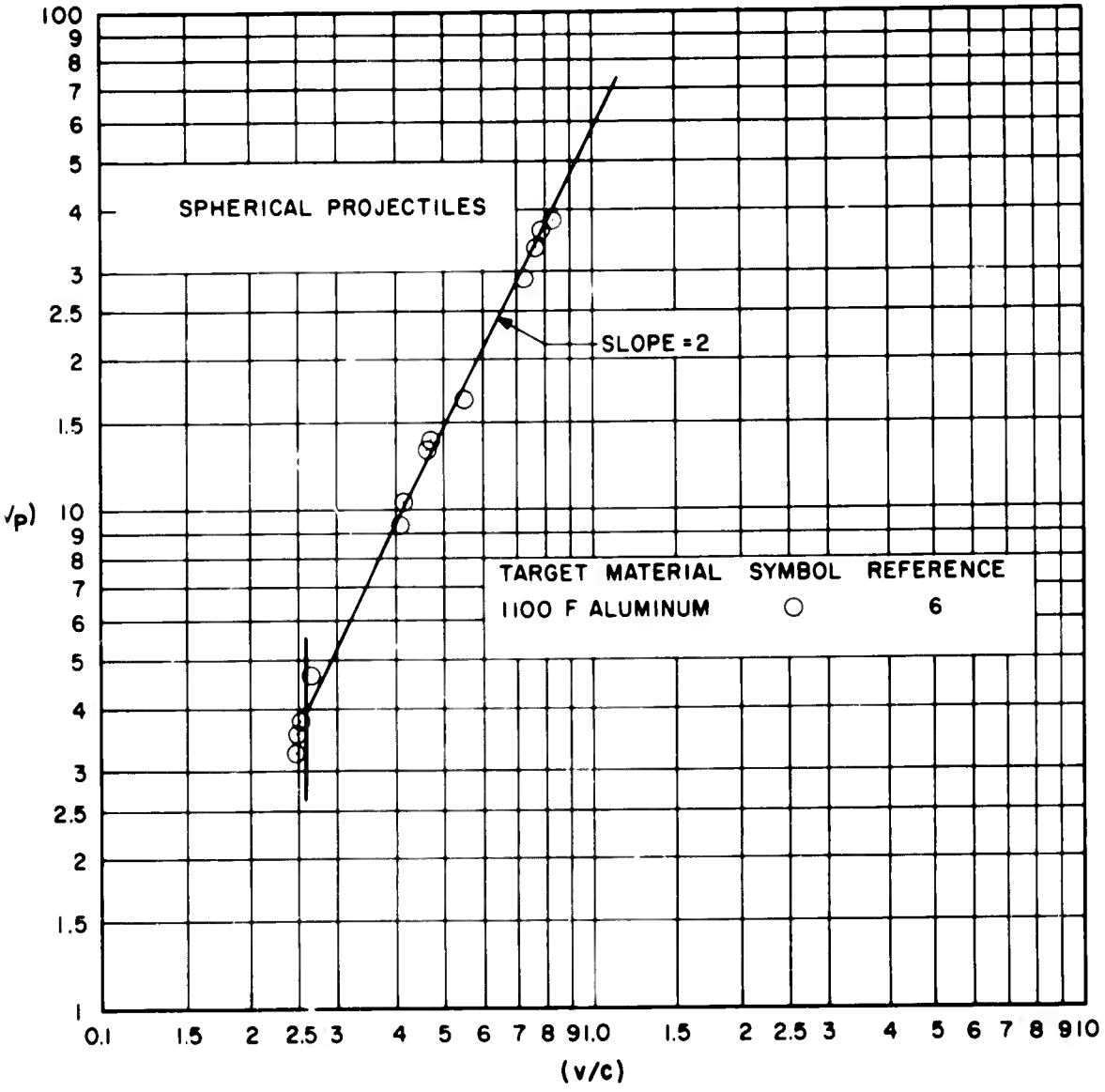

VARIATION OF CRATER VOLUME PARAMETER WITH IMPACT VELOCITY PARAMETER FOR ALUMINUM ALLOY PROJECTILES AND TARGETS

FIGURE - 15b

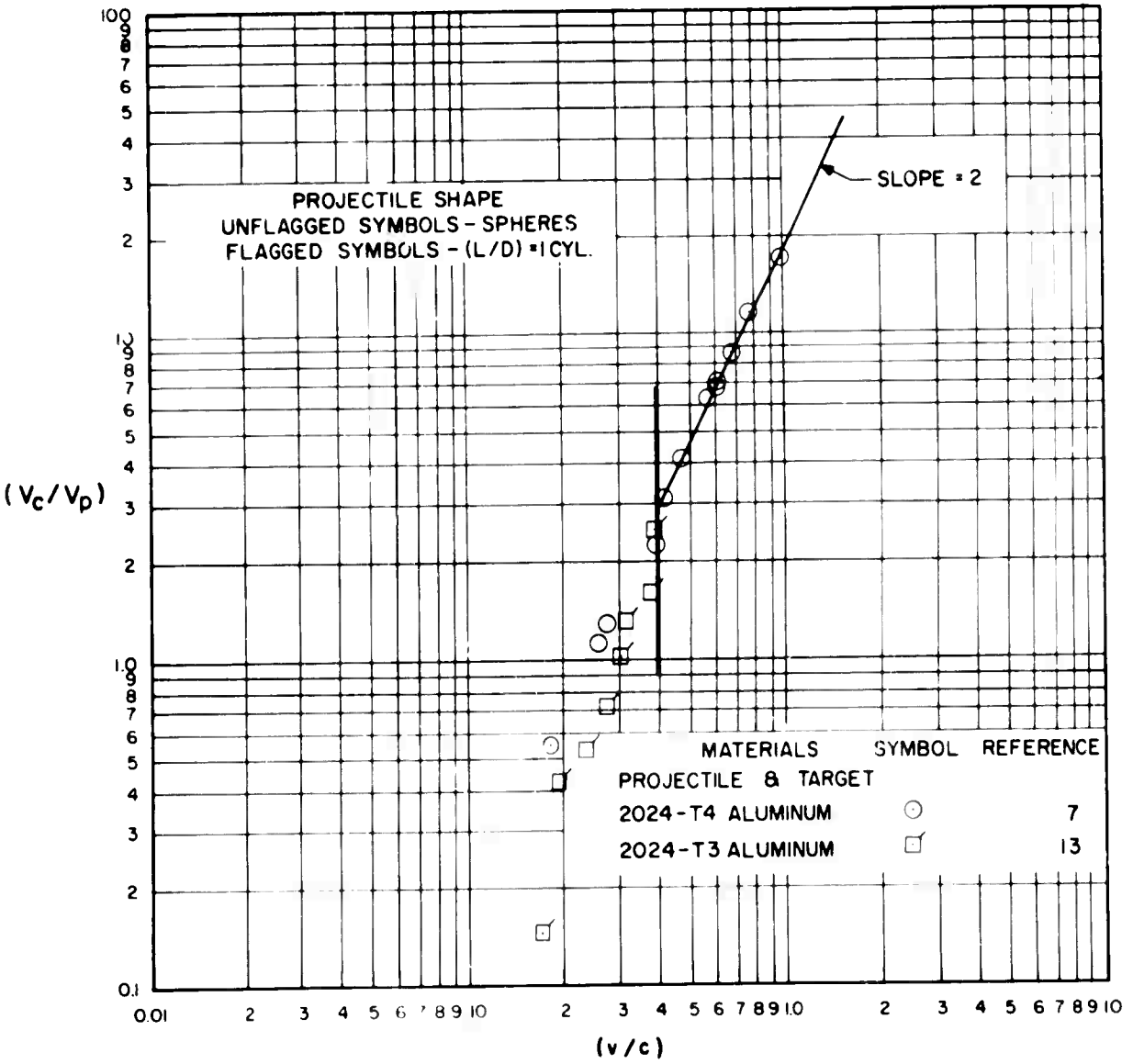

VARIATION OF CRATER VOLUME PARAMETER WITH IMPACT VELOCITY PARAMETER FOR ZINC PROJECTILES AND TARGETS

FIGURE - 16a

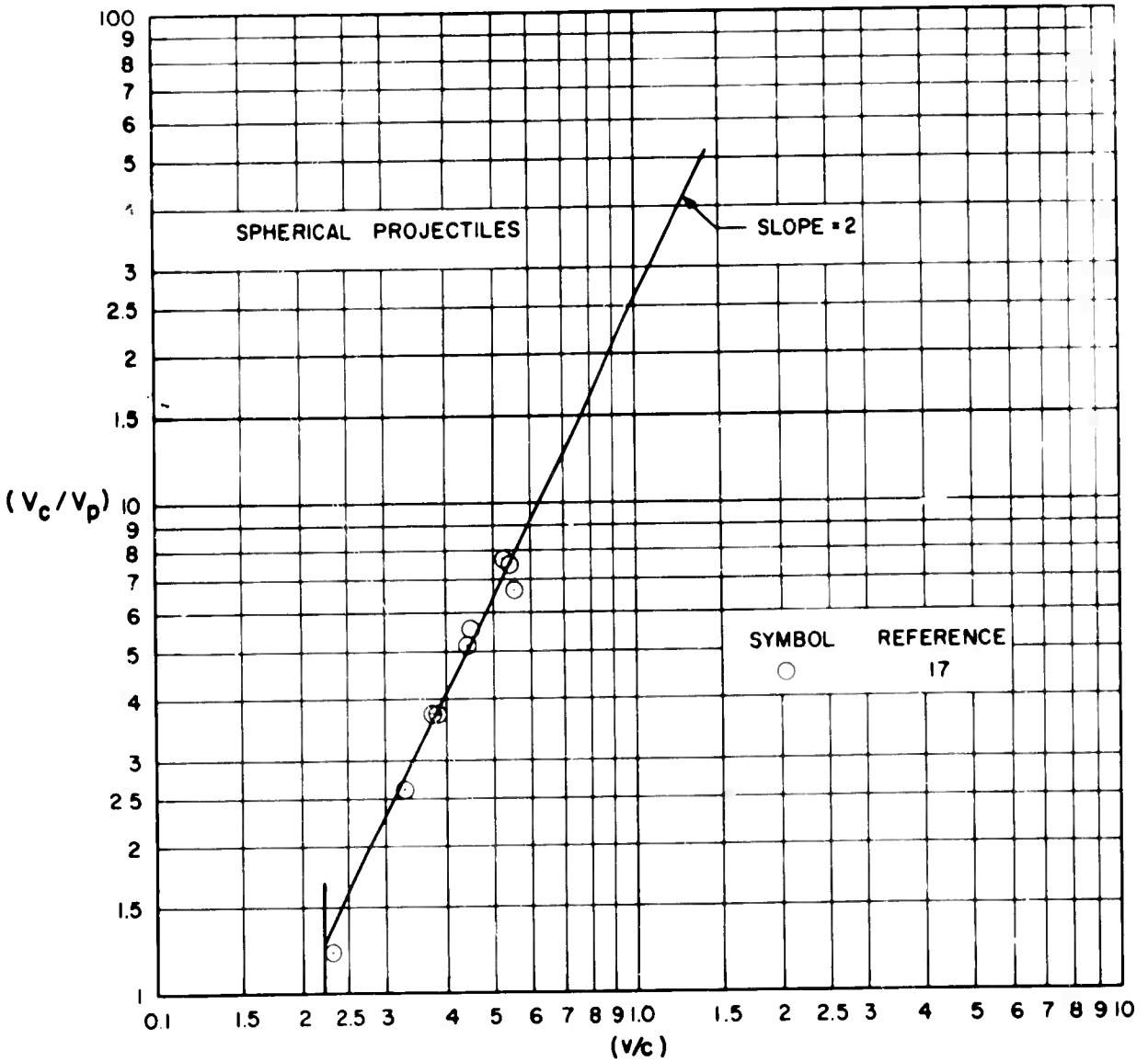

VARIATION OF CRATER VOLUME PARAMETER WITH IMPACT VELOCIT
PARAMETER FOR STEEL PROJECTILES AND ZINC TARGETS

FIGURE-16b

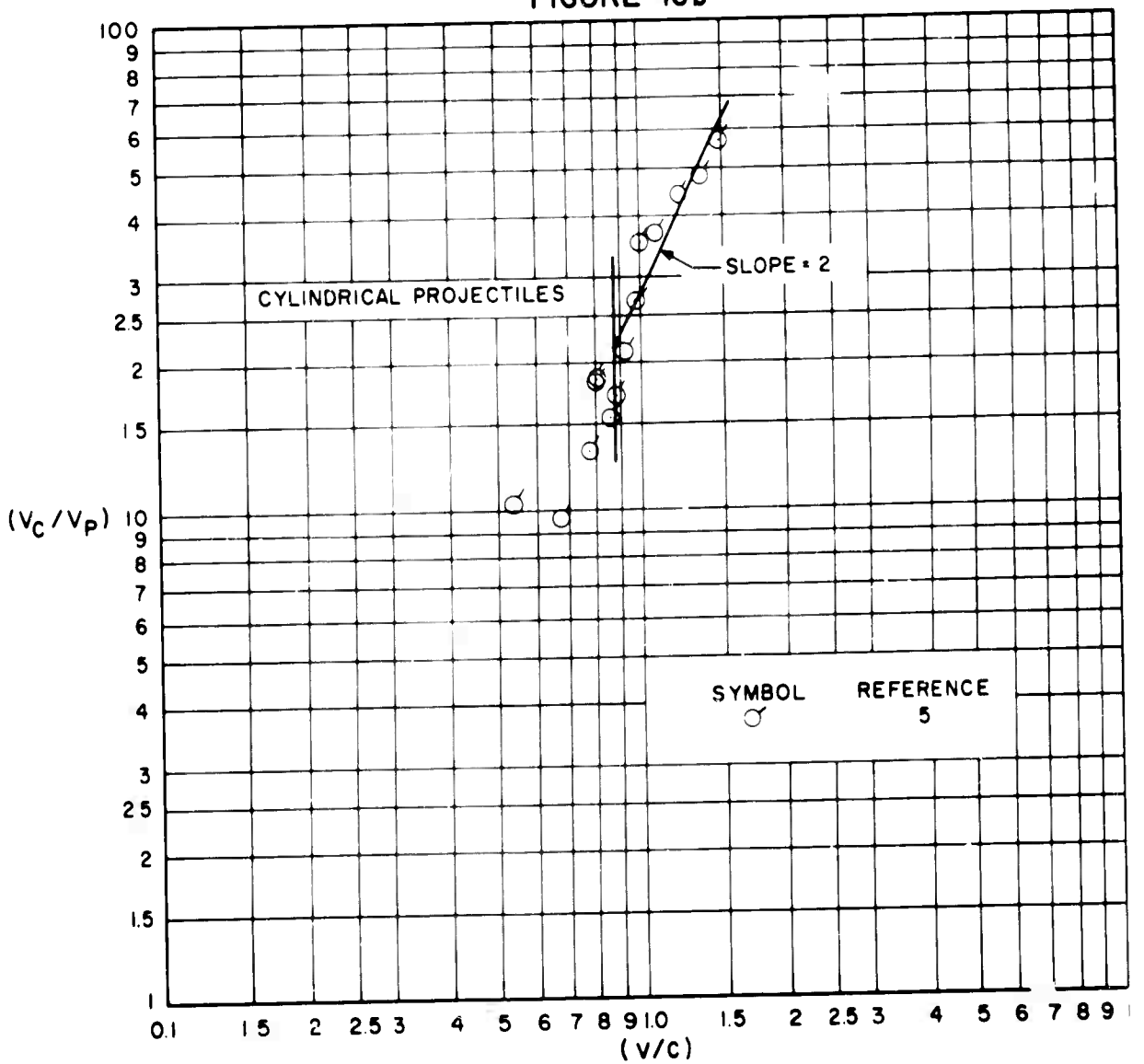

VARIATION OF CRATER VOLUME PARAMETER WITH IMPACT VELOCITY PARAMETER FOR TIN PROJECTILES AND TARGETS

FIGURE - 17

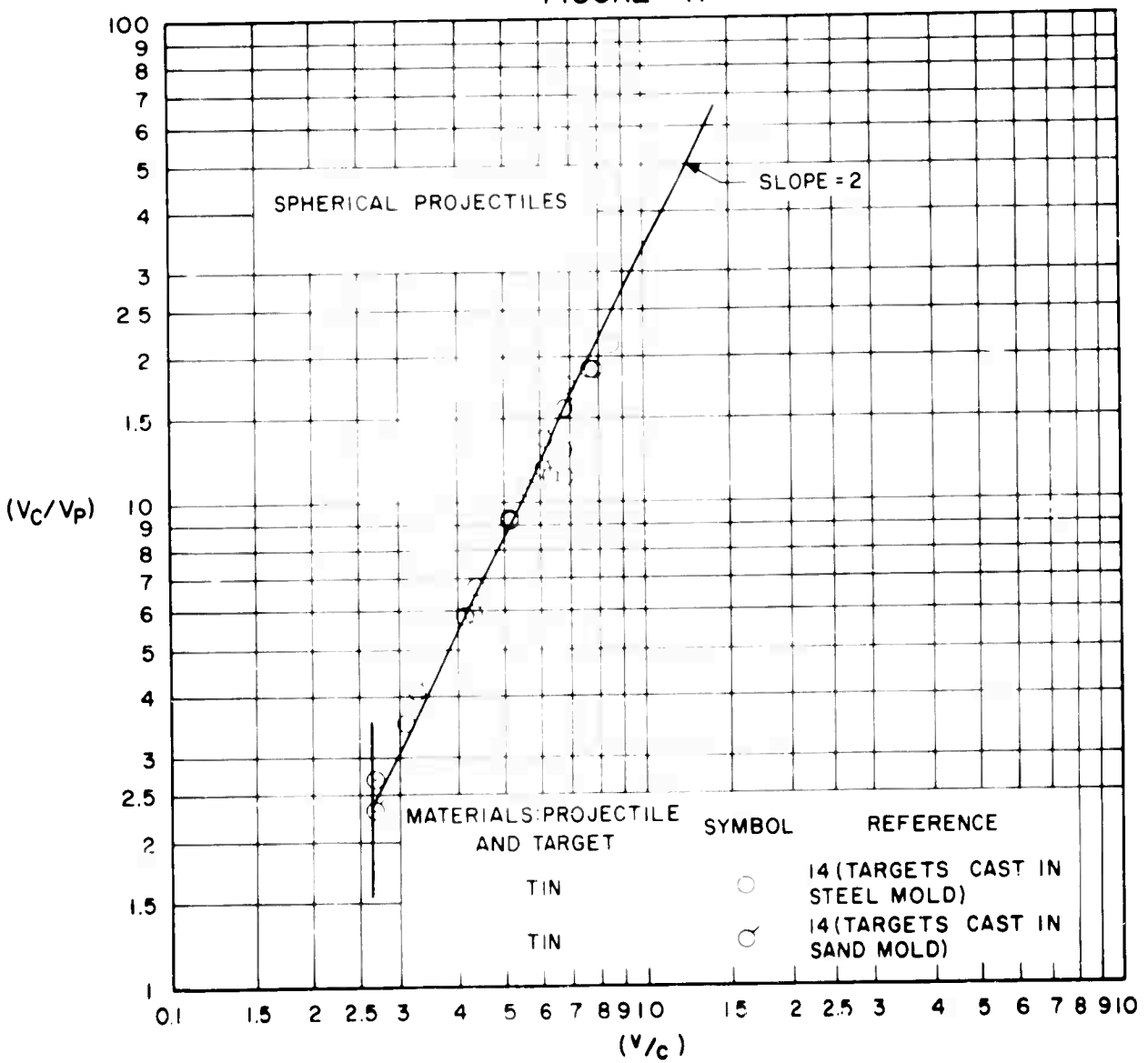

VARIATION OF CRATER VOLUME PARAMETER WITH IMPACT VELOCITY PARAMETER FOR STEEL PROJECTILES AND TARGETS

FIGURE - 18

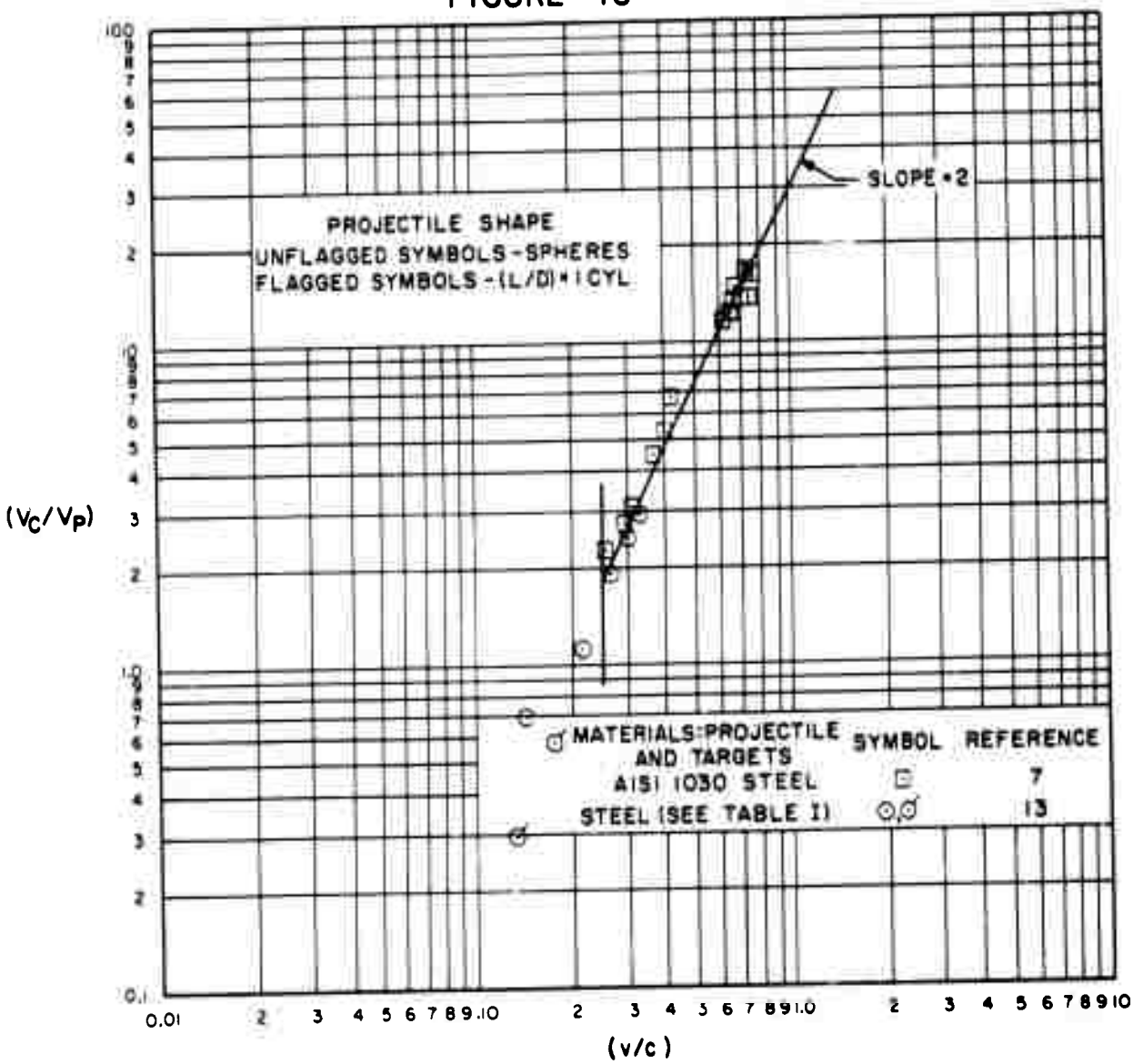

VARIATION OF CRATER VOLUME PARAMETER WITH IMPACT VELOCITY PARAMETER FOR STEEL PROJECTILES AND CADMIUM TARGETS

FIGURE - 19

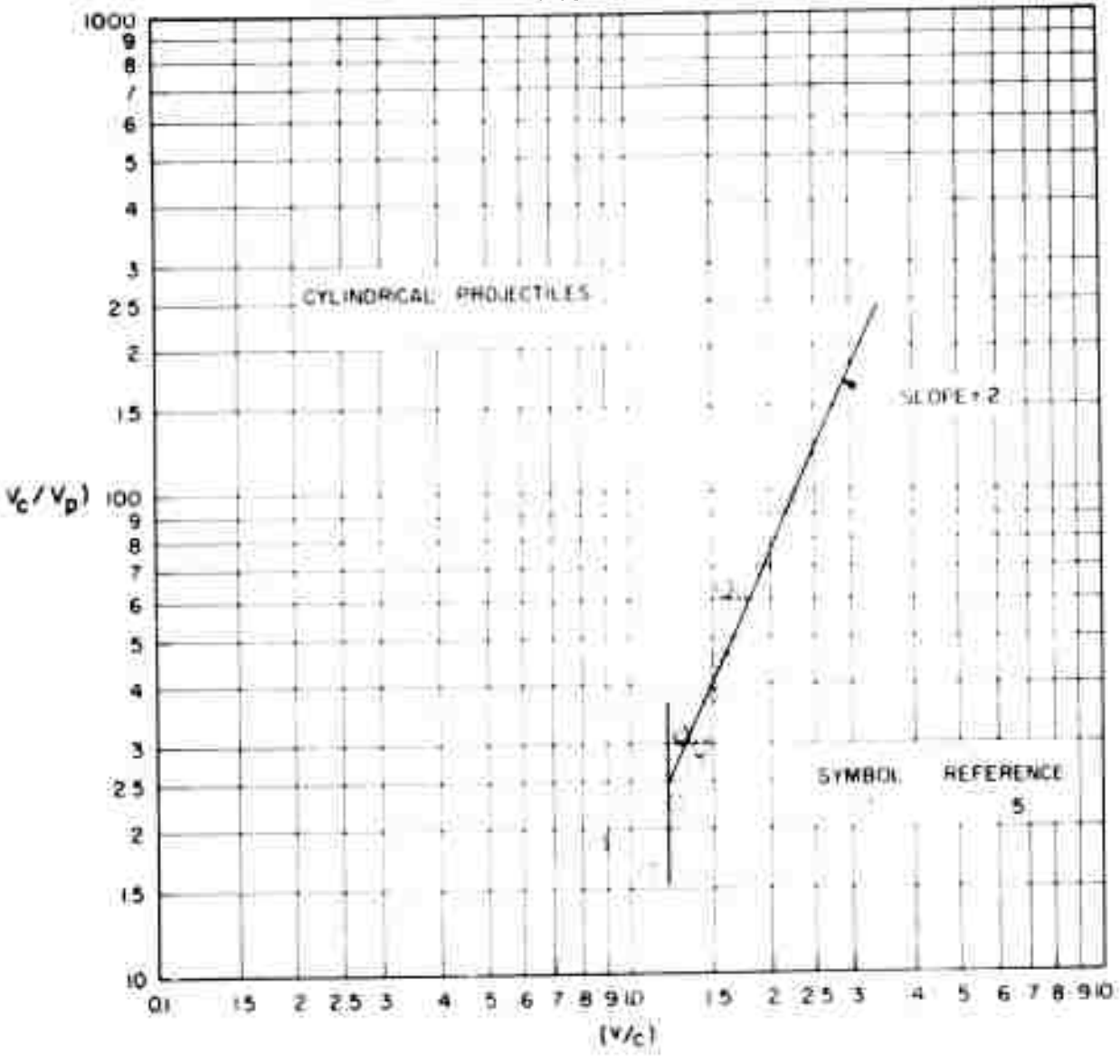

VARIATION OF CRATER VOLUME PARAMETER WITH IMPACT VELOCITY PARAMETER FOR ALUMINUM ALLOY PROJECTILES AND COPPER TARGETS

FIGURE-20a

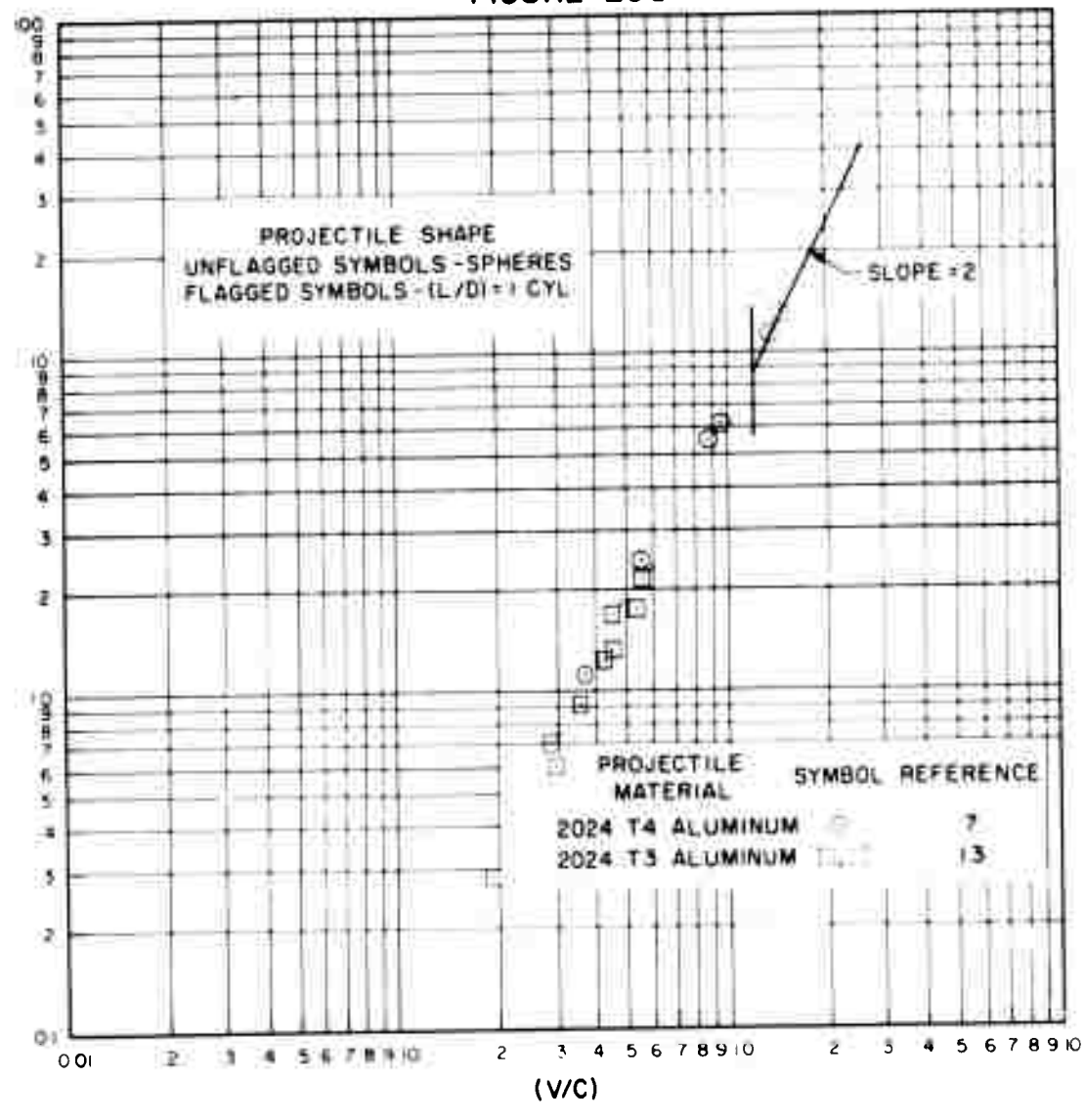

VARIATION OF CRATER VOLUME PARAMETER WITH IMPACT VELOCITY PARAMETER FOR STEEL PROJECTILES AND COPPER TARGETS

FIGURE - 20b

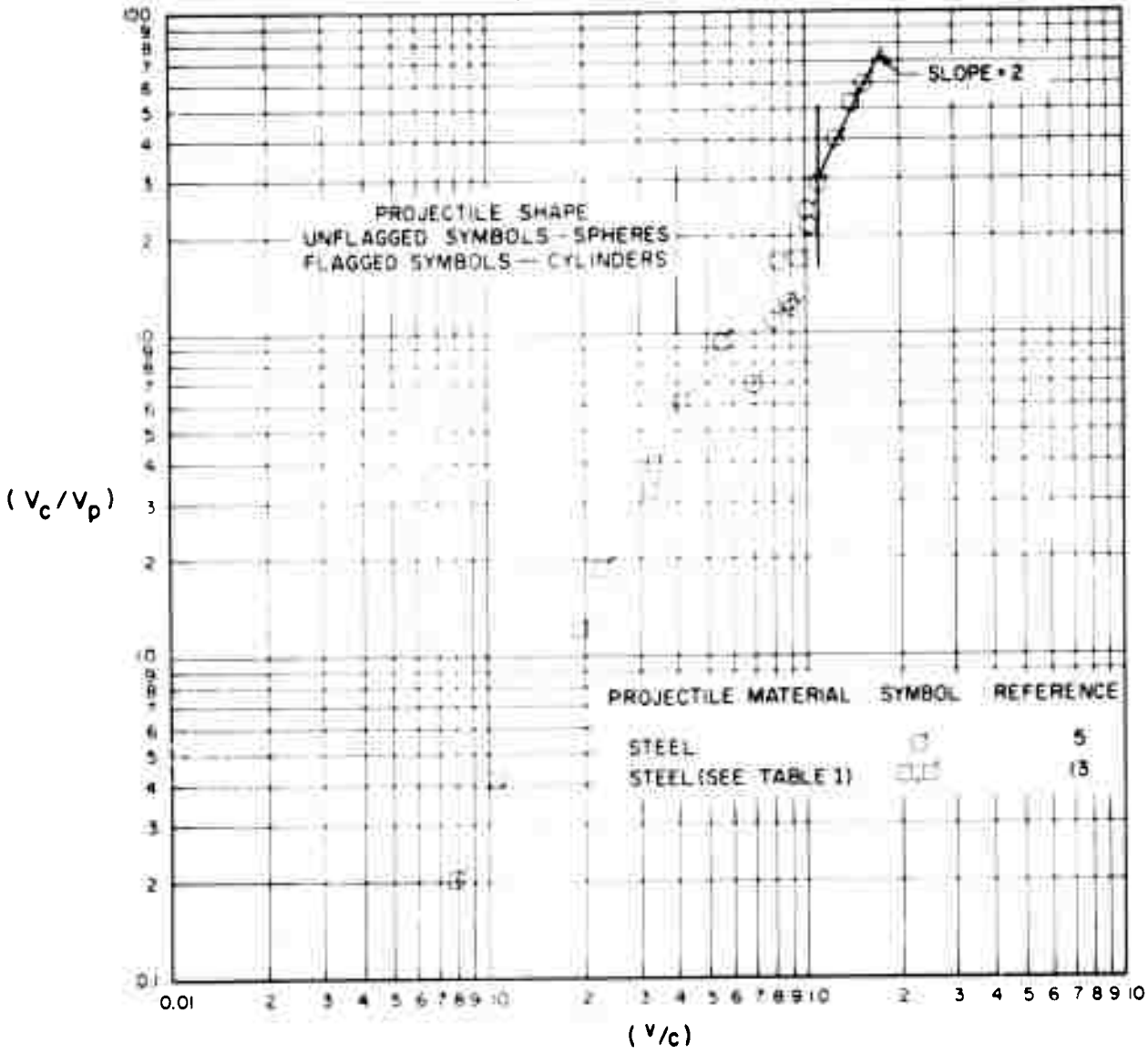

'ARIATION OF CRATER VOLUME PARAMETER WITH IMPACT VELOCITY PARAMETER FOR COPPER PROJECTILES AN) TARGETS

FIGURE - 20c

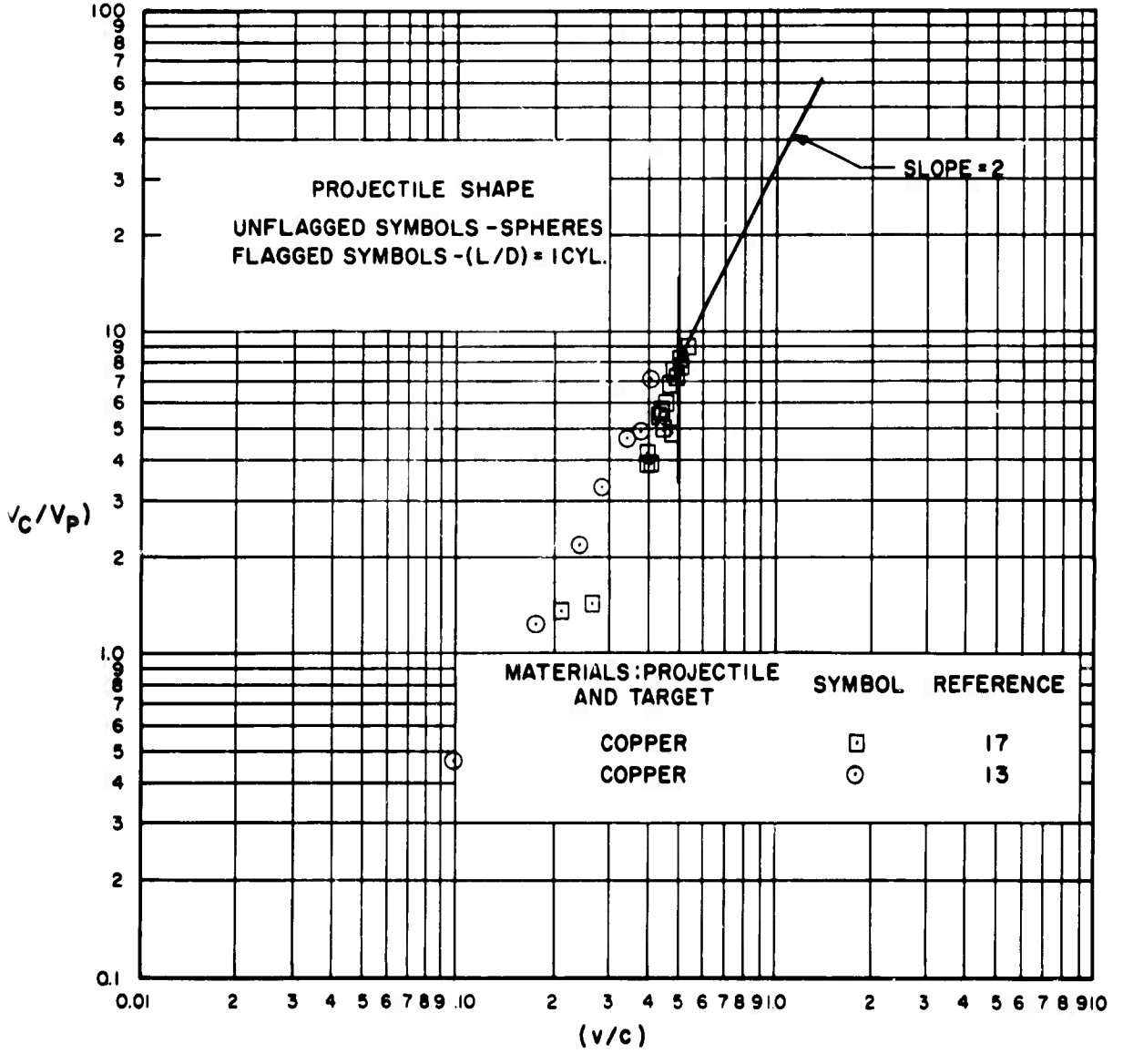

VARIATION OF CRATER VOLUME PARAMETER WITH IMPACT VELOCITY PARAMETER FOR ALUMINUM ALLOY PROJECTILES AND LEAD TARGETS

FIGURE-21a

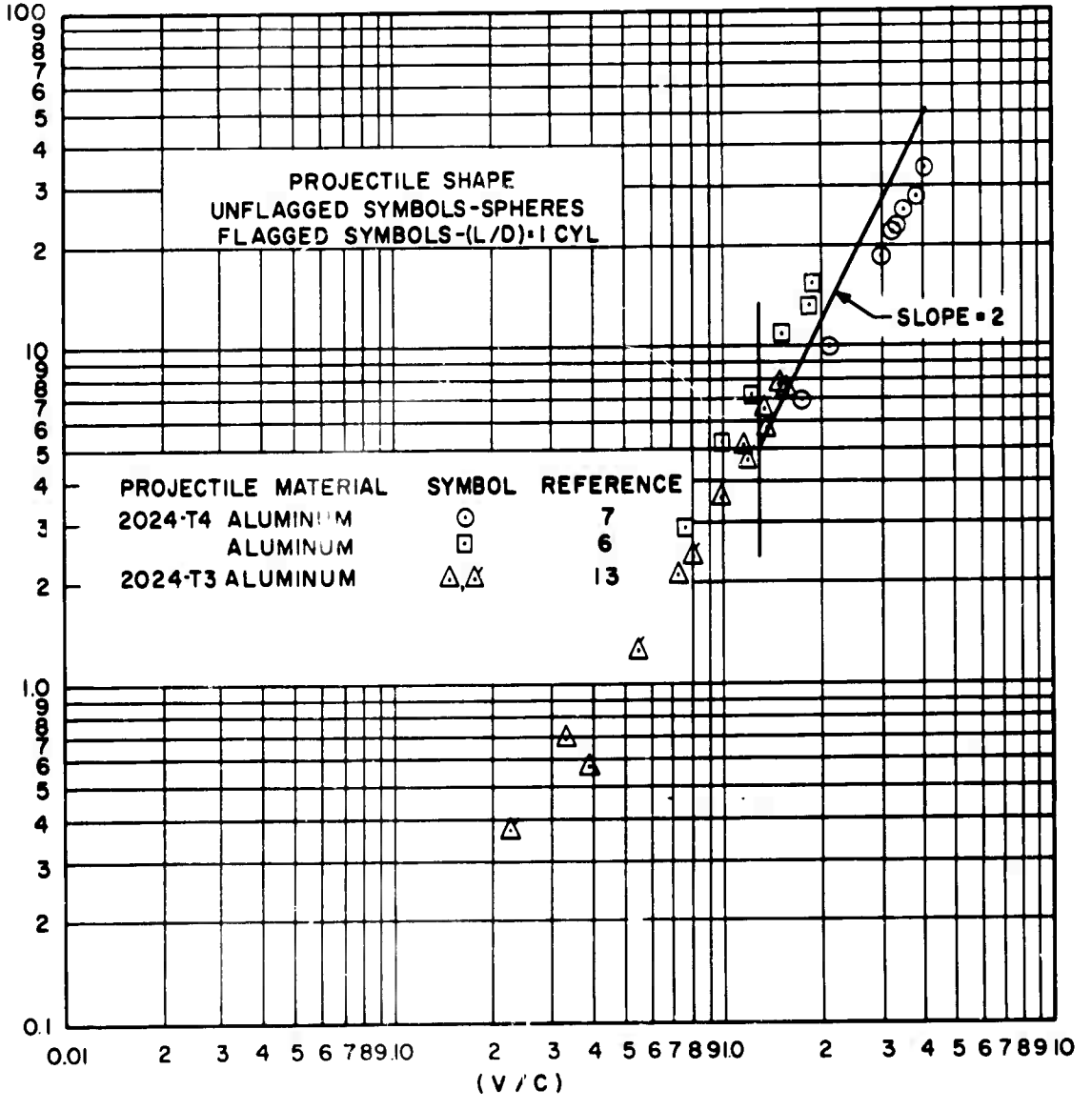

VARIATION OF CRATER VOLUME PARAMETER WITH IMPACT VELOCITY PARAMETER FOR STEEL PROJECTILES AND LEAD TARGETS

FIGURE - 21b

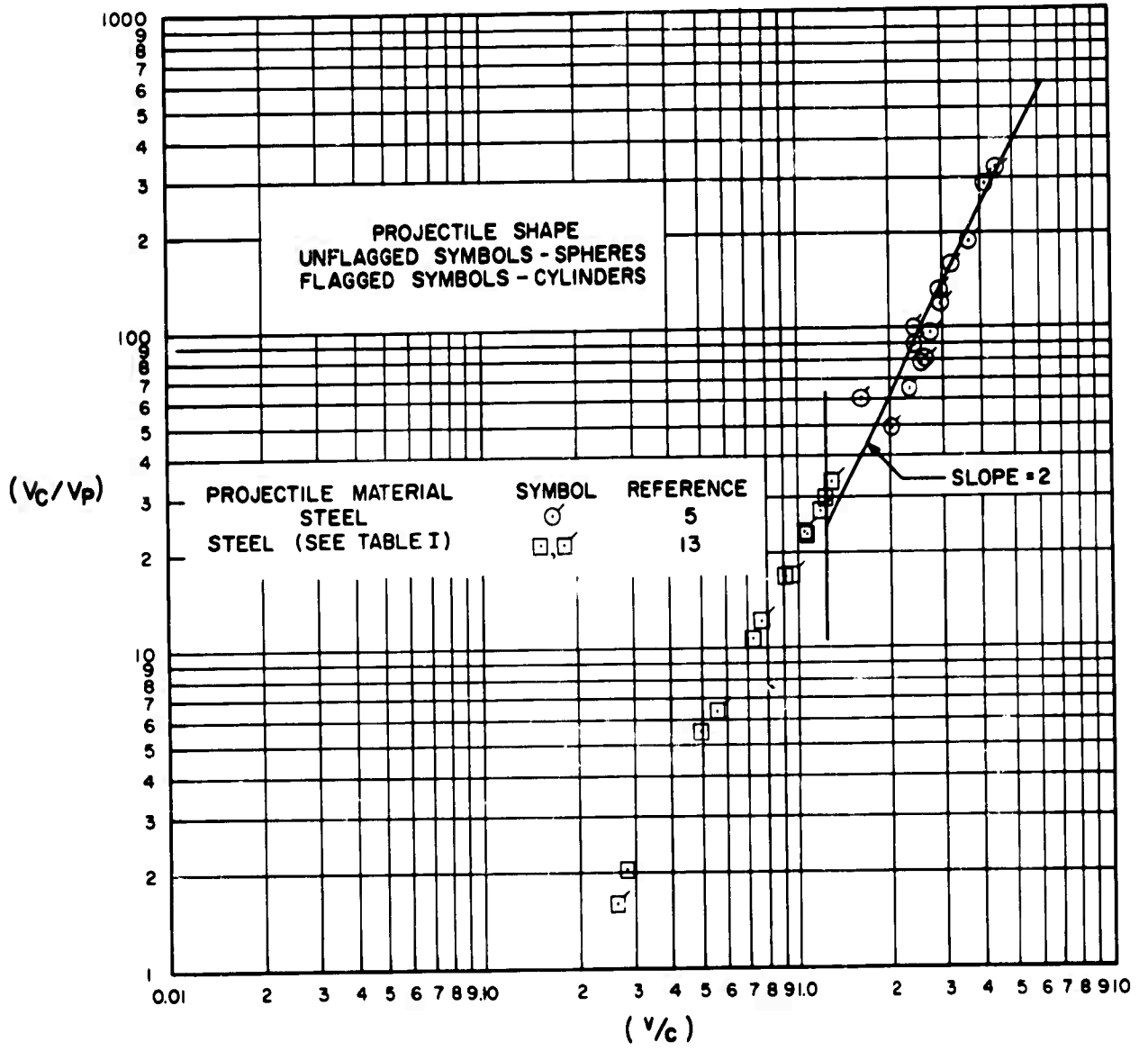

VARIATION OF CRATER VOLUME PARAMETER WITH IMPACT VELOCITY PARAMETER FOR COPPER PROJECTILES AND LEAD TARGETS

FIGURE - 21c

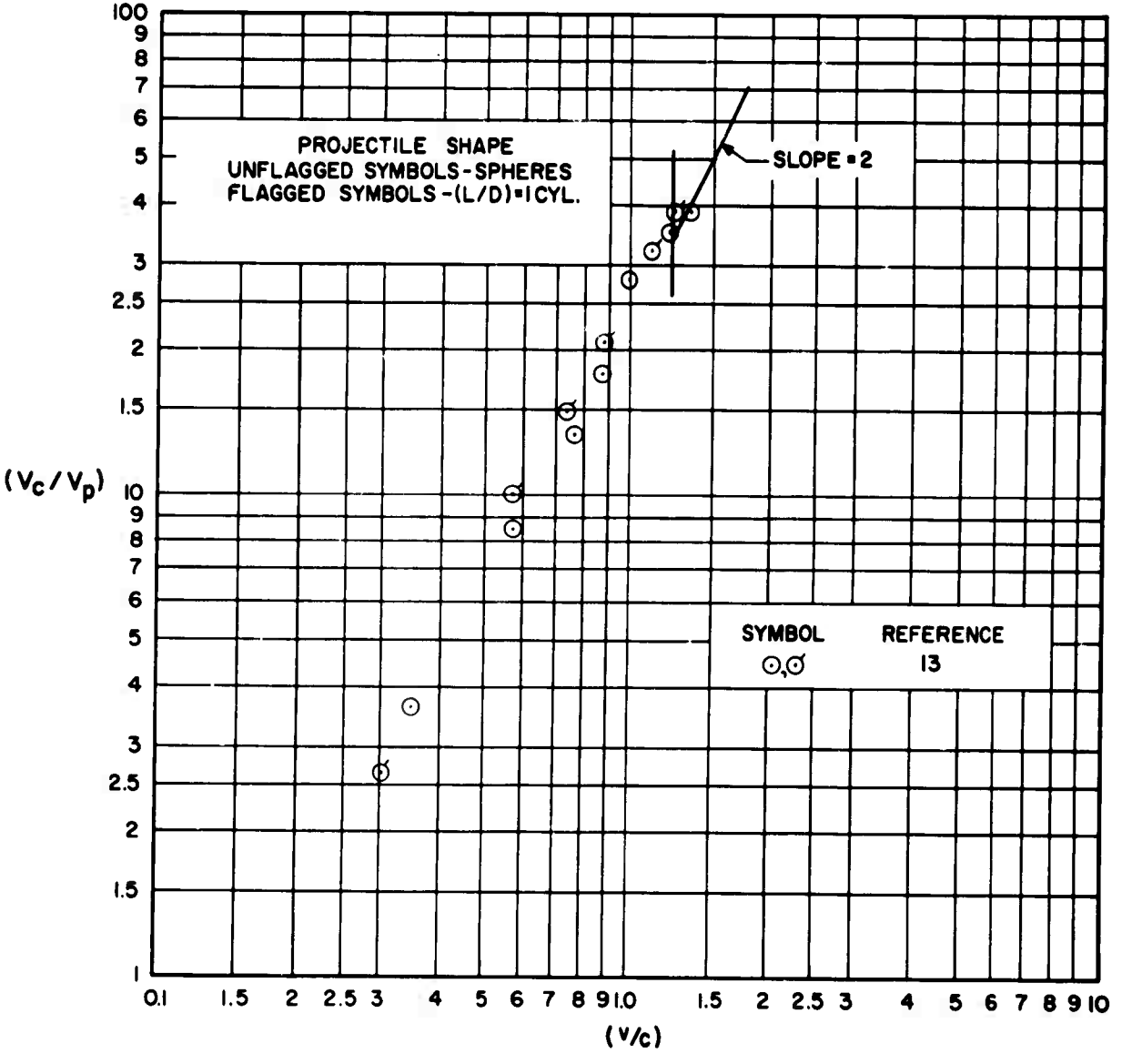

VARIATION OF CRATER VOLUME PARAMETER WITH IMPACT VELOCITY PARAMETER FOR LEAD PROJECTILES AND TARGETS

FIGURE - 21d

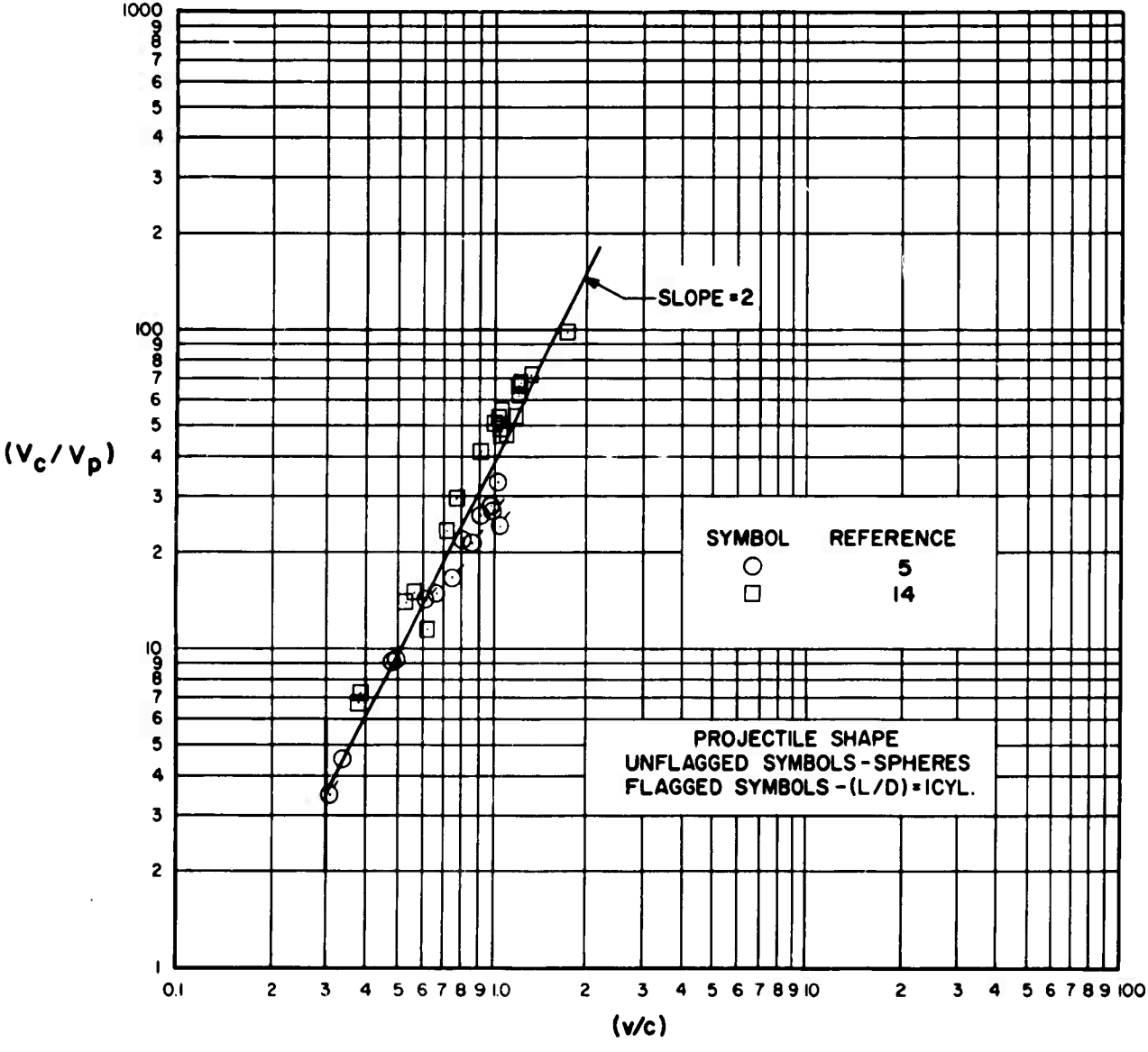

EFFECT OF TARGET DENSITY ON CRATER VOLUME

FIGURE-22

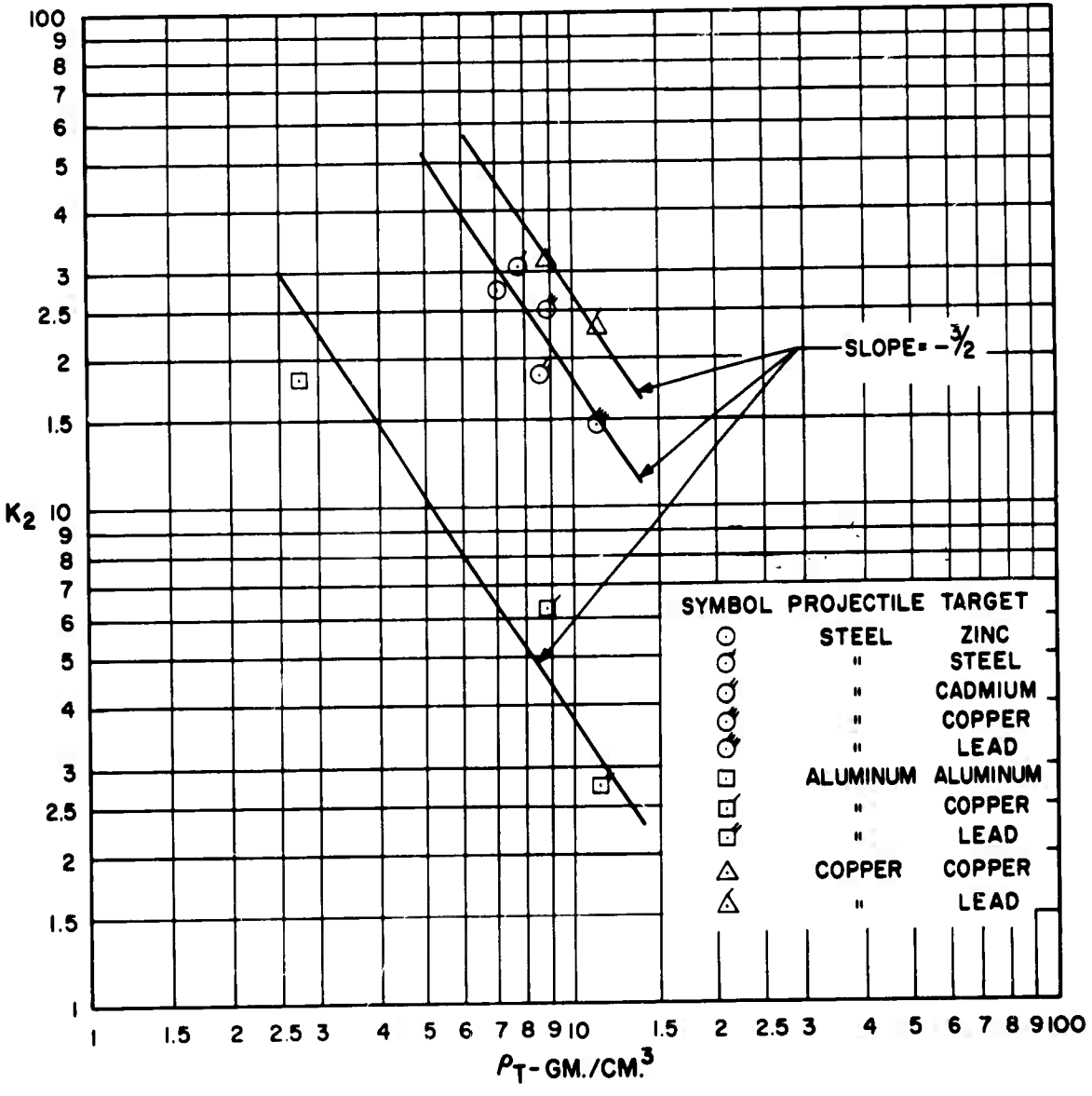

EFFECT OF PROJECTILE DENSITY ON CRATER VOLUME

FIGURE - 23

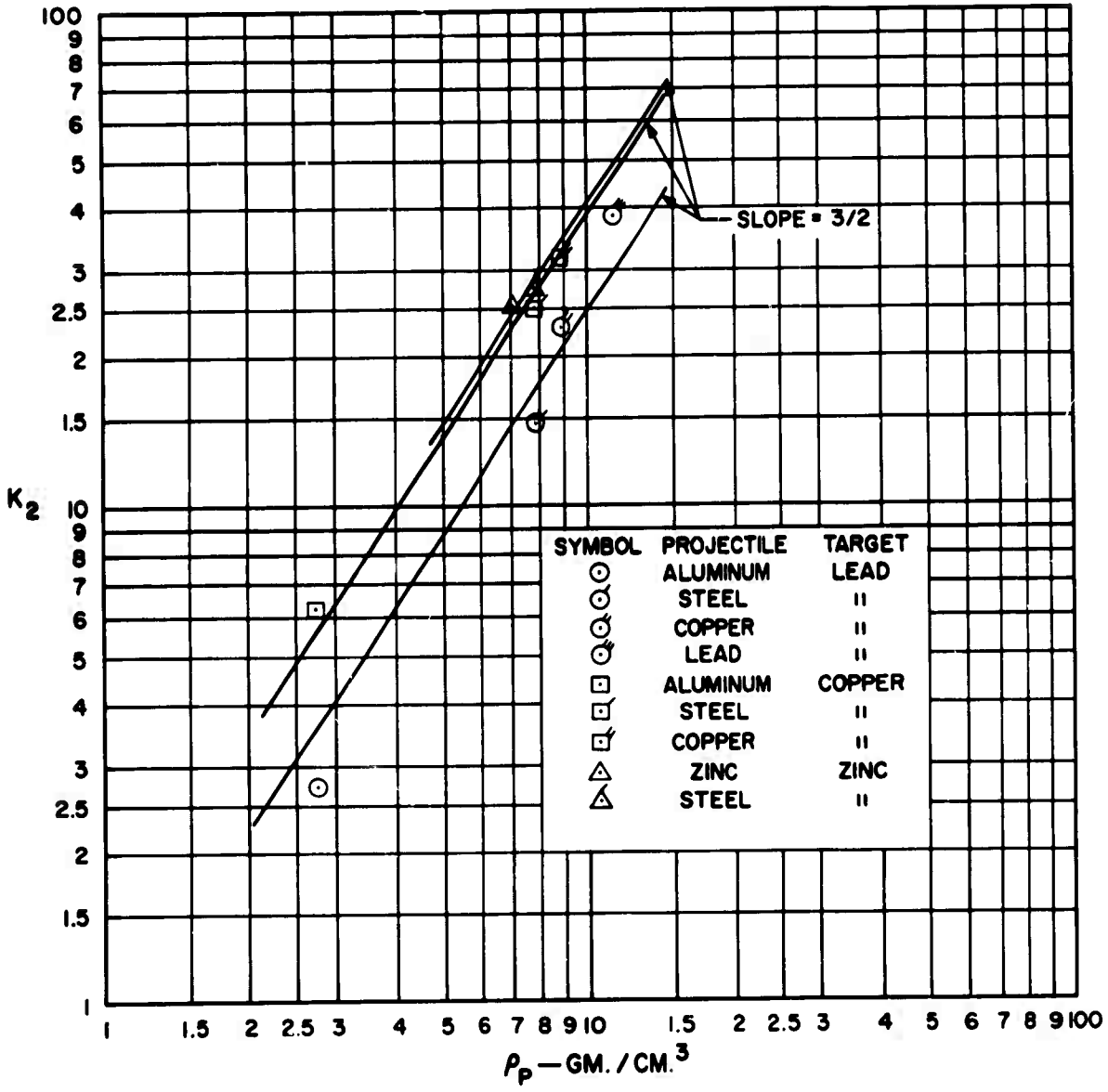

EFFECT OF TARGET DENSITY ON PENETRATION

FIGURE - 24

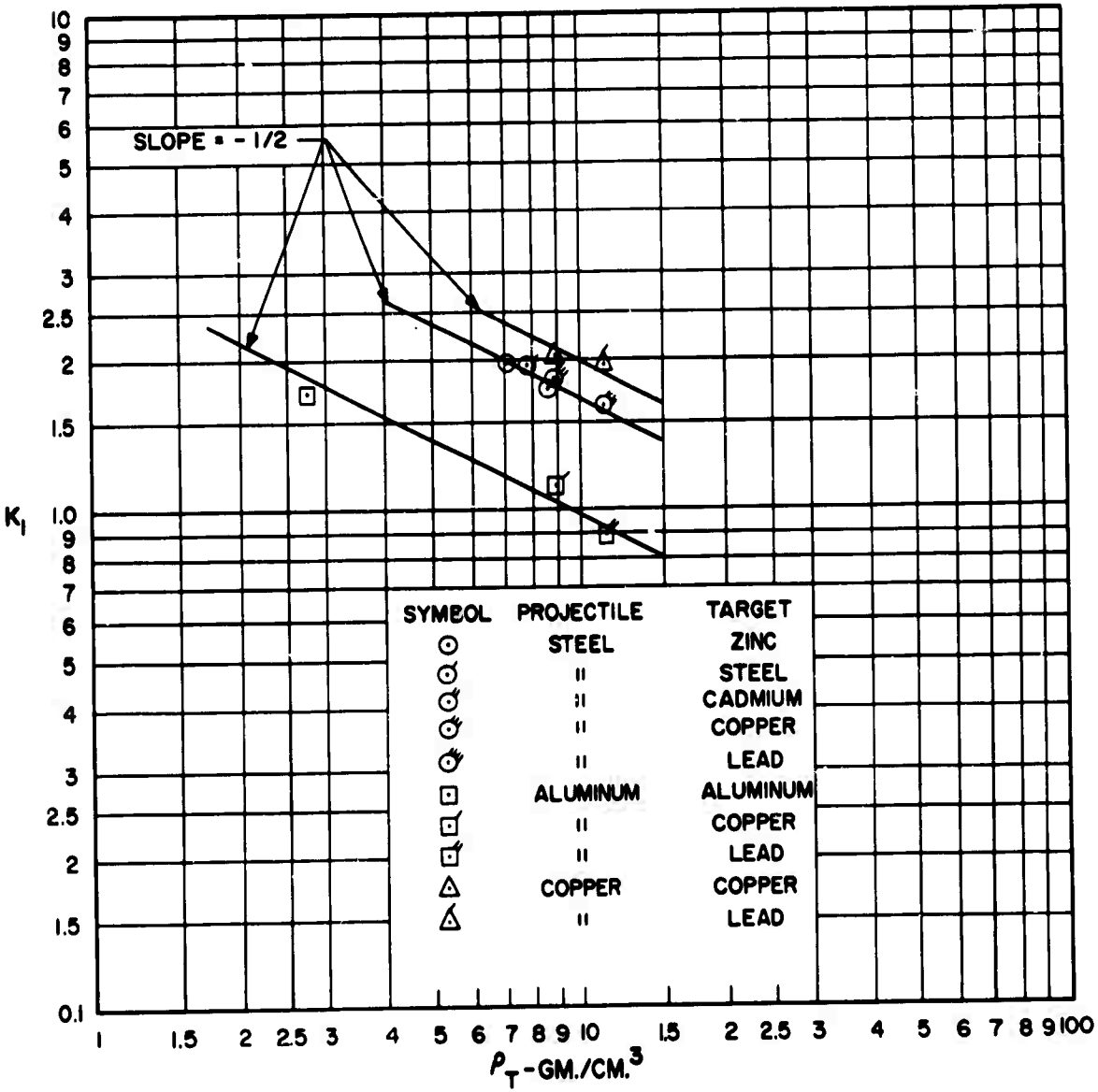

EFFECT OF PROJECTILE DENSITY ON PENETRATION

FIGURE-25

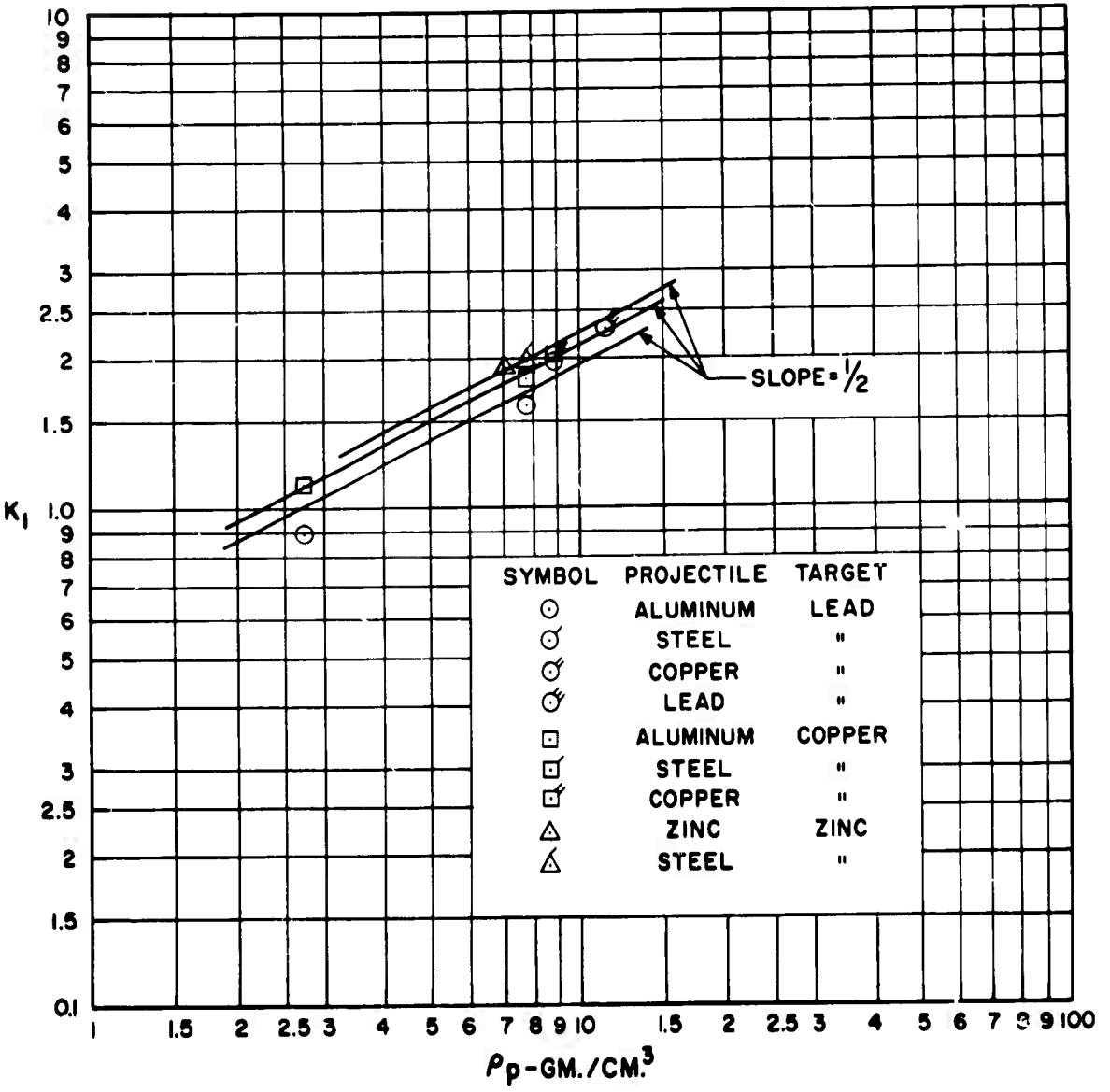

COMPARISON OF PREDICTED PENETRATION WITH TEST DATA

FIGURE-26a

$$\left[P_C / D_S\right]_{(\frac{V}{C})=1} = K_1$$

TEST DATA

$$\left[P_C / D_S\right]_{(\frac{V}{C})=1} = 1.96\,(\rho_P/\rho_T)^{1/2}$$

EQN. 8

SEE TABLE I FOR KEY TO SYMBOLS

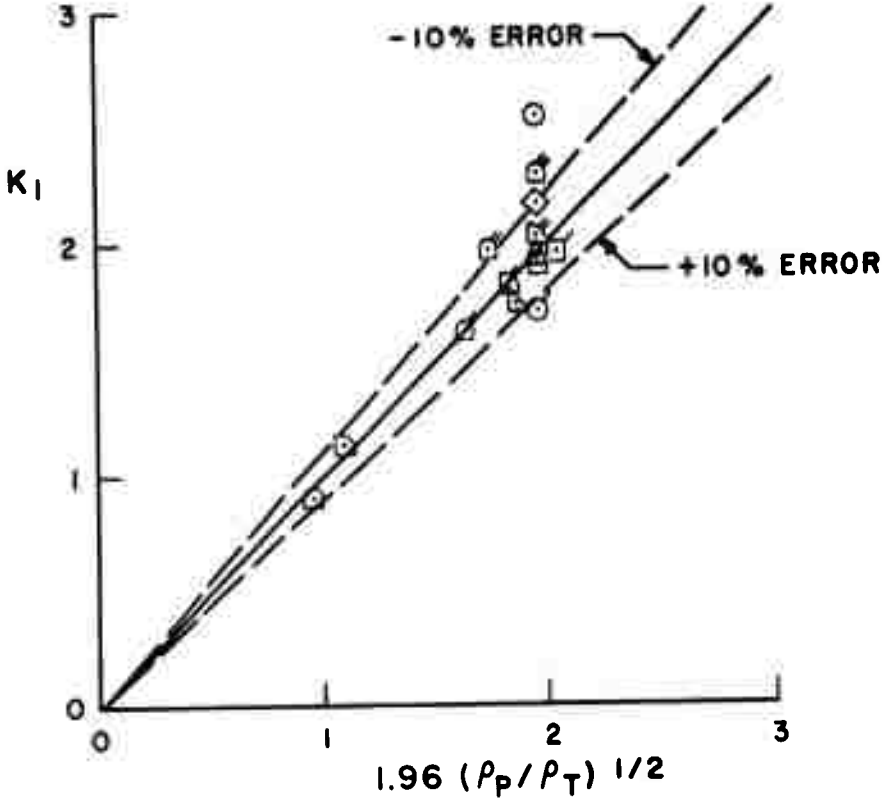

COMPARISON OF PREDICTED PENETRATION WITH TEST DATA
FIGURE - 26b

$$\left[P_C/D_S\right]_{\left(\frac{V}{C}\right)=1} = K_1$$

TEST DATA

$$\left[P_C/D_S\right]_{\left(\frac{V}{C}\right)=1} = 2.28\,(\rho_P/\rho_T)^{2/3}$$

EQN. 1

SEE TABLE I FOR KEY TO SYMBOLS

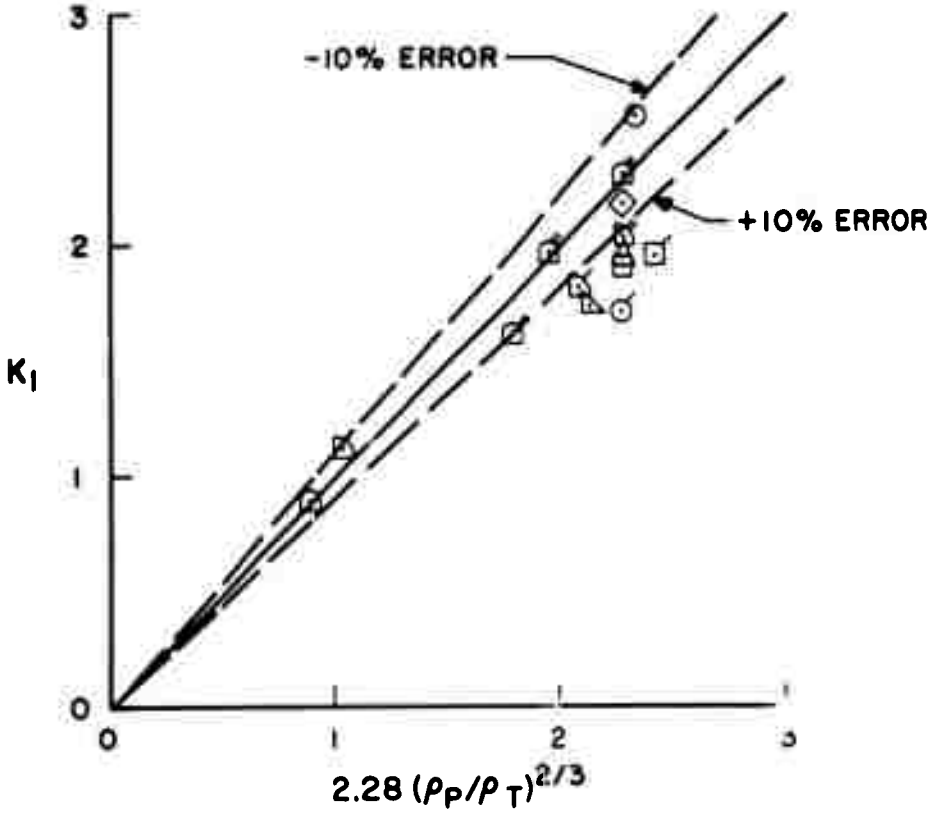

COMPARISON OF PREDICTED CRATER VOLUME WITH TEST DATA

FIGURE-27a

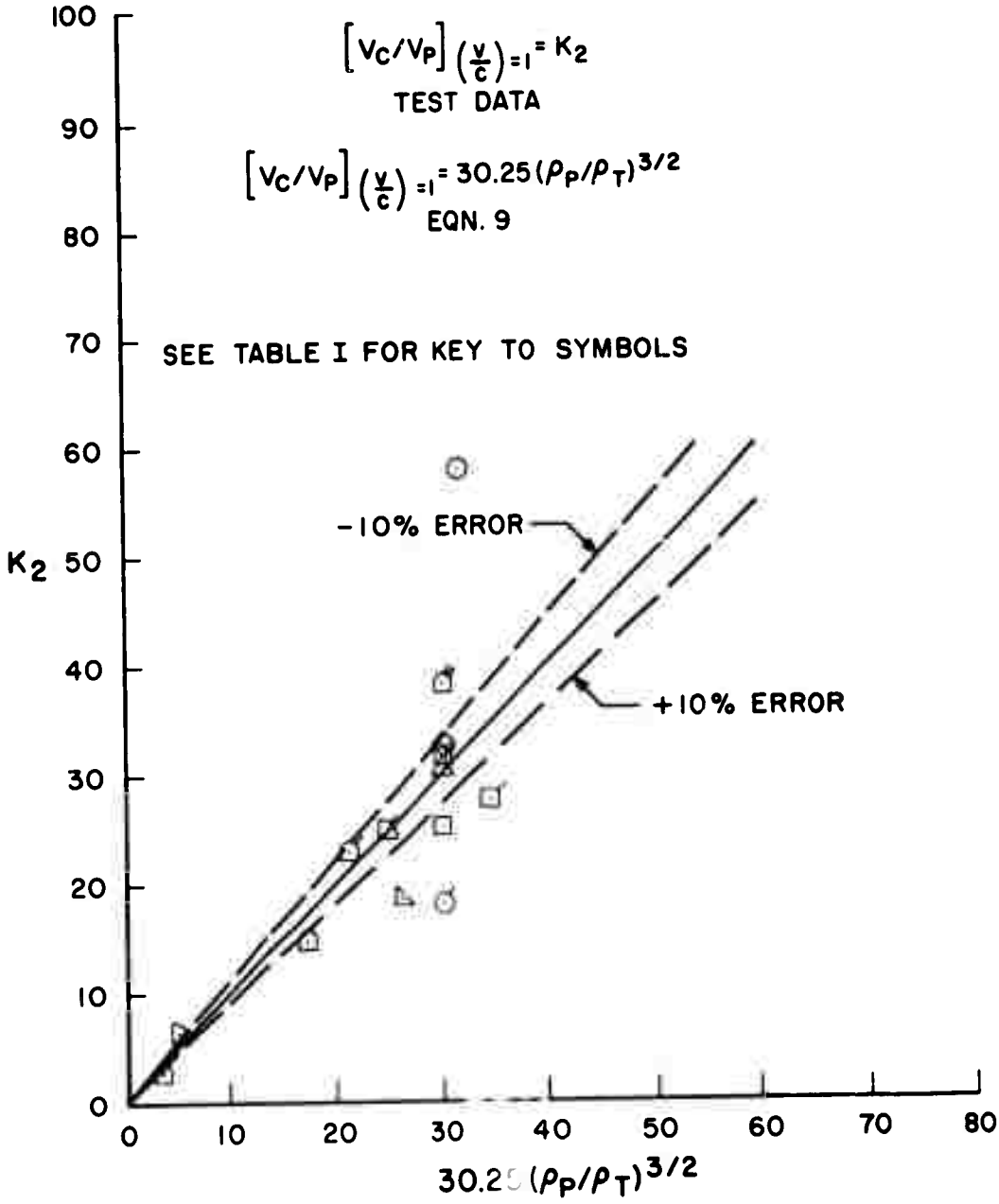

COMPARISON OF PREDICTED CRATER VOLUME WITH TEST DATA

FIGURE - 27b

$$\left[V_C/V_P\right]_{\frac{v}{c}=1} = K_2$$

TEST DATA

$$\left[V_C/V_P\right]_{\frac{v}{c}=1} = 34\,(\rho_P/\rho_T)^{3/2}$$

EQN. 2

SEE TABLE I FOR KEY TO SYMBOLS

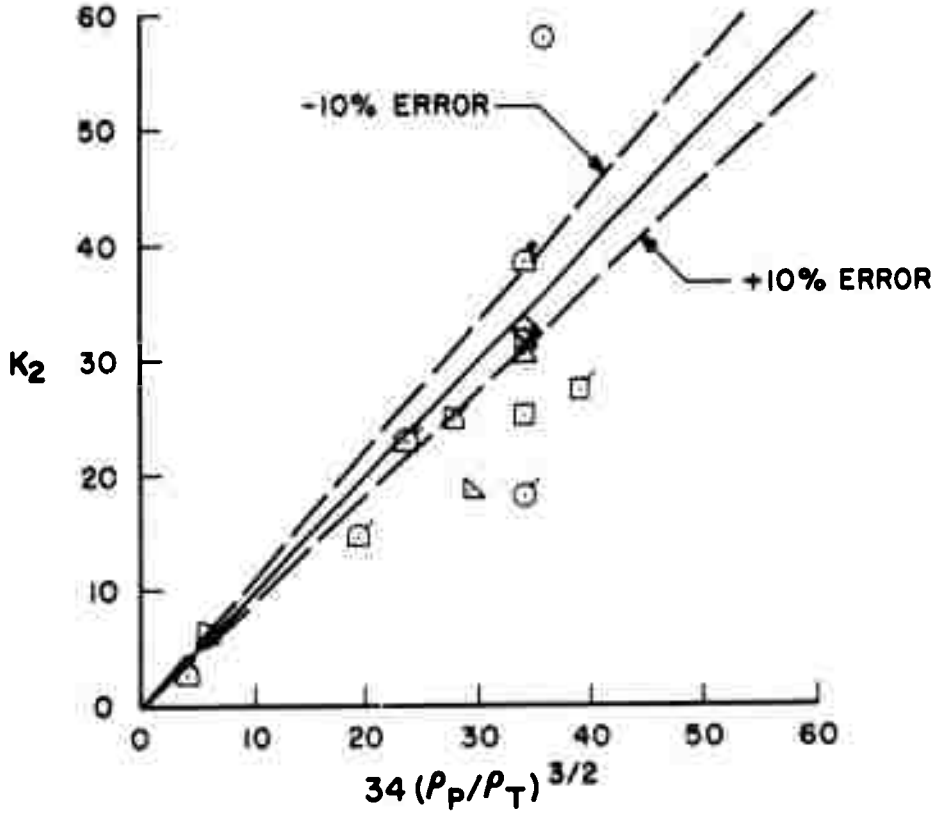

BLANK PAGE

VARIATION OF CRATER PROFILE PARAMETER WITH IMPACT VELOCITY FOR NORMAL AND OBLIQUE INCIDENCE STEEL PROJECTILES AND LEAD TARGETS

FIGURE-28

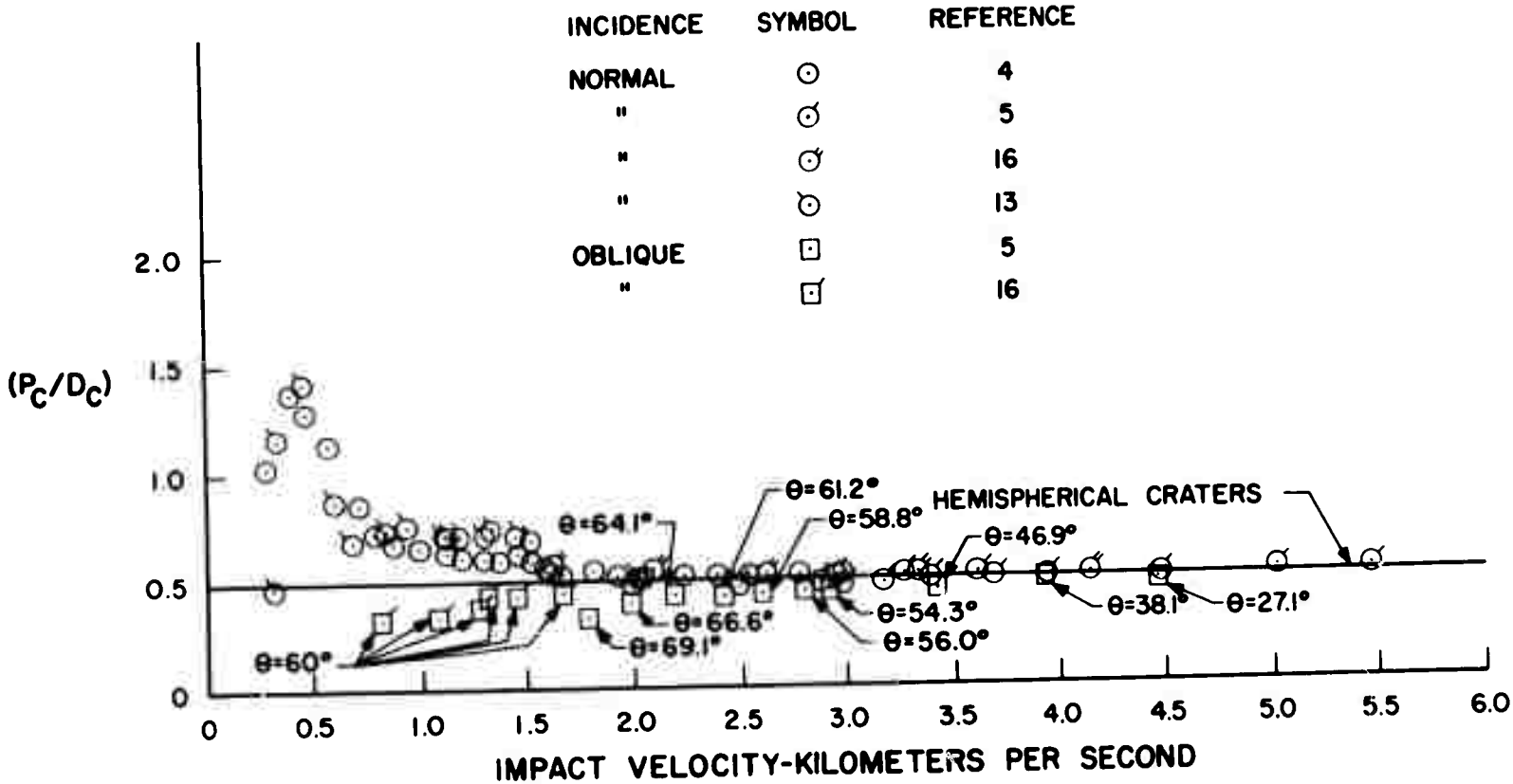

VARIATION OF CRATER SHAPE PARAMETER WITH IMPACT VELOCITY FOR OBLIQUE INCIDENCE STEEL PROJECTILES AND LEAD TARGETS

FIGURE-29

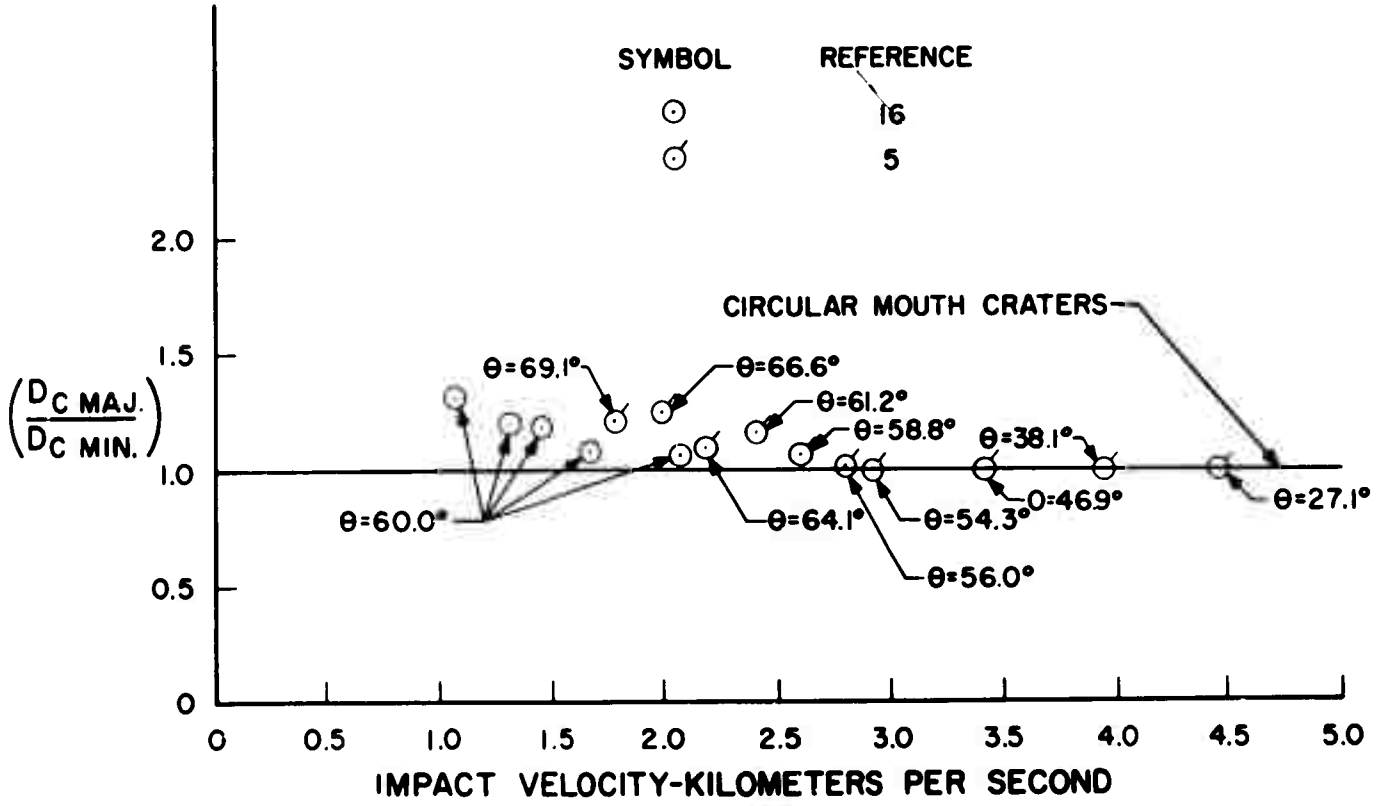

VARIATION OF PENETRATION PARAMETER WITH IMPACT VELOCITY PARAMETER FOR NORMAL AND OBLIQUE INCIDENCE-COPPER PROJECTILES AND TARGETS

FIGURE-30

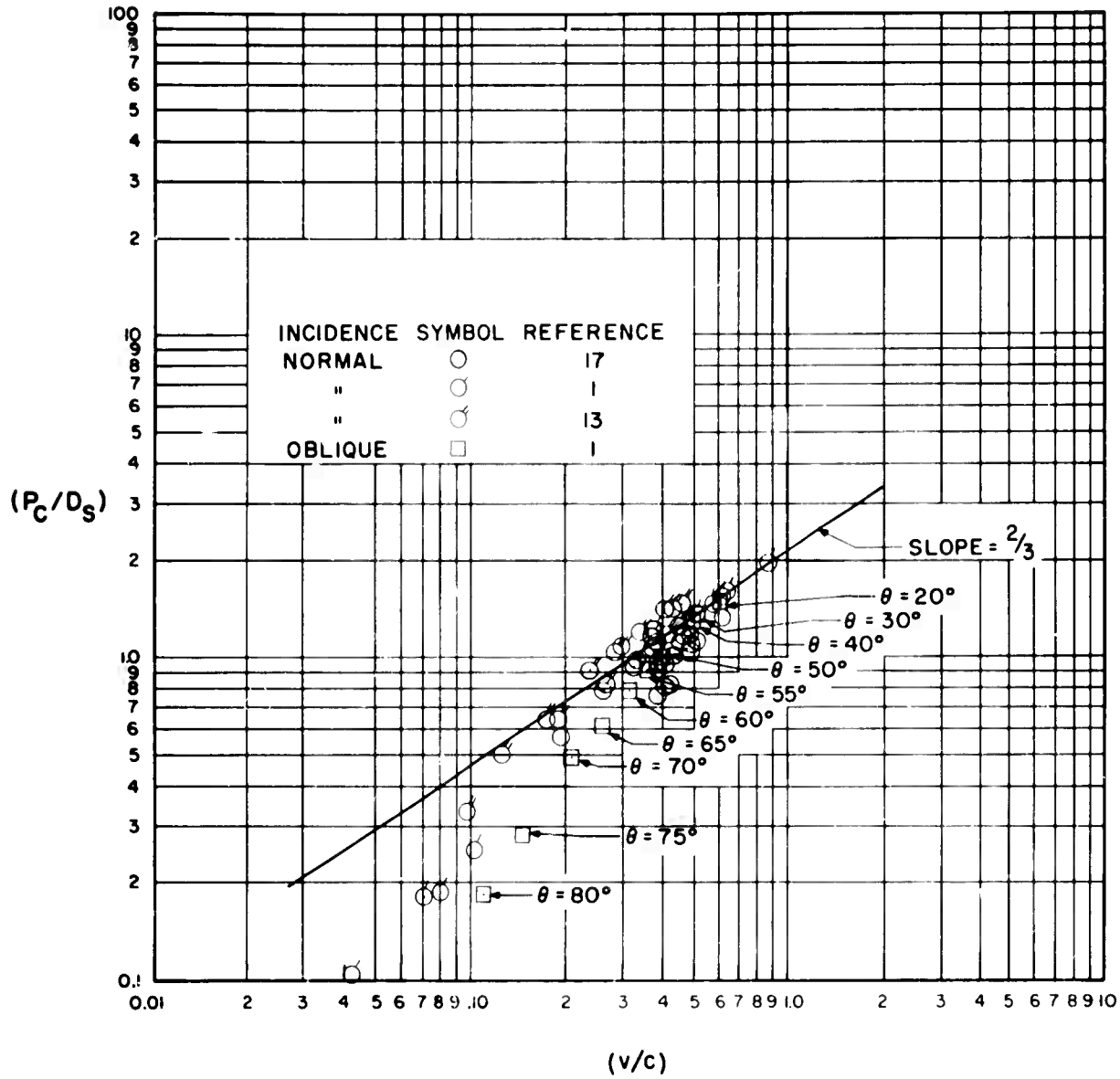

VARIATION OF PENETRATION PARAMETER WITH IMPACT VELOCITY PARAMETER FOR NORMAL AND OBLIQUE INCIDENCE-STEEL PROJECTILES AND LEAD TARGETS

FIGURE 31

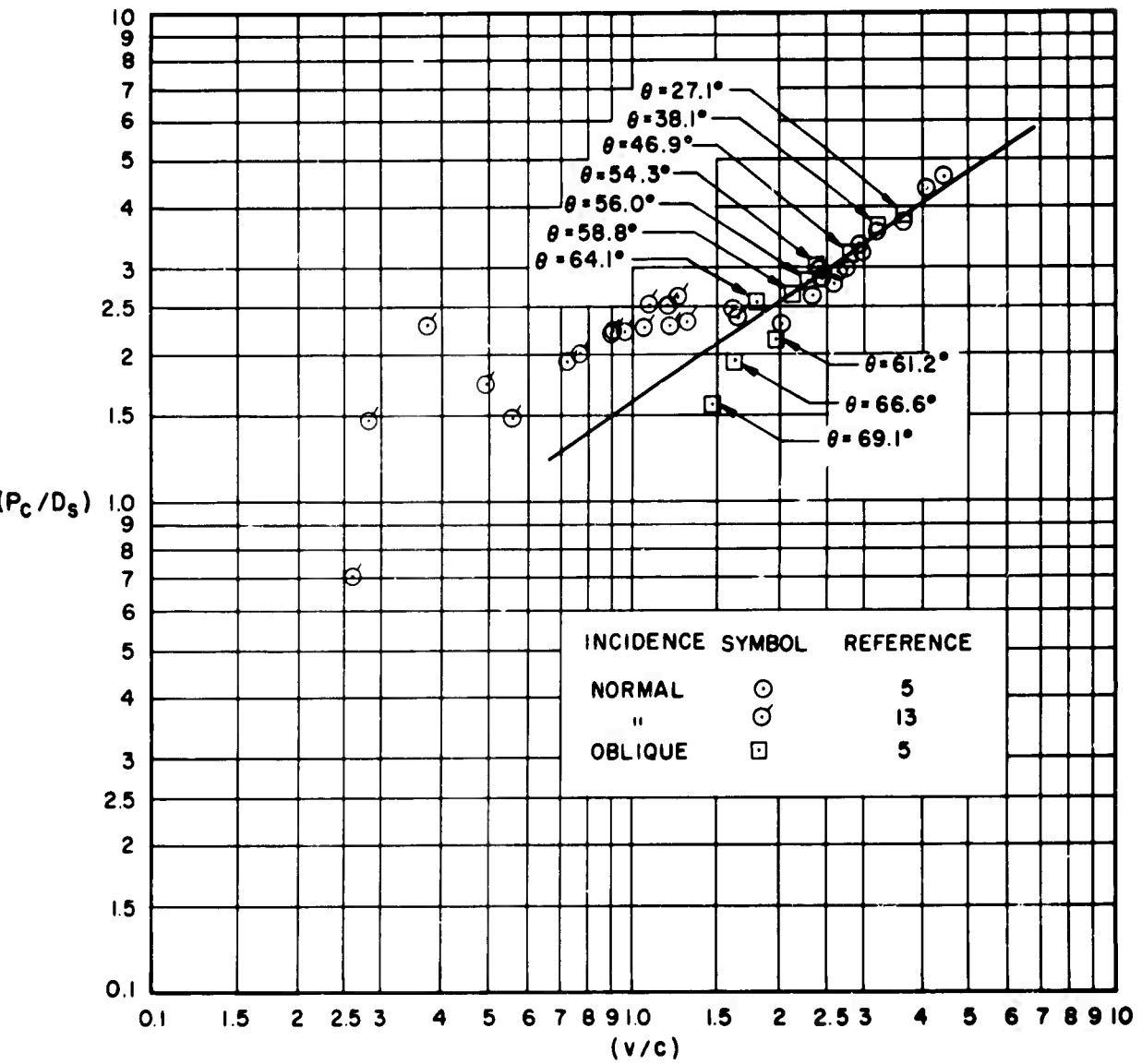

TABLE I SUMMARY OF PROJECTILE, TARGET, AND PROJECTILE-TARGET SYSTEM PROPERTIES

PROJECTILE			TARGET			SYSTEM				
SIZE & SHAPE	MATERIAL	ρ_P gm./cm.^{3}	MATERIAL	ρ_T gm./cm.^{3}	c km./sec.	ρ_P ρ_T	K_1	K_2	REFERENCE	SYMBOL ON FIGURES 26 & 27
3/8-in. dia. sphere	Aluminum	2.81	1100 F Aluminum	2.71	5.041	1.037	2.55	57.94	6	○
0.2 & 0.4-in. dia. sphere; 0.0620 & 0.22-in. dia. sphere & 0.22 & 0.55-in. dia. (L/D) = 1 cylinders.	2024-T4 Aluminum, 2024-T3 Aluminum	2.77	Same as projectile	2.77	5.105	1	1.71	18.12	7,13	○
3/16-in. dia. sphere	Zinc	7.13	Same as projectile	7.13	3.670	1	1.91	25.02	17	□
0.375, 0.500, 0.625, & 1.000-in. dia. (L/D) = 0.267, 0.08&0.14, 0.72, & 0.064 & 0.10 cylinders.	Steel	7.83	Zinc	7.13	3.670	1.098	1.96	27.45	5	□
3/16-in. dia. sphere	Tin	7.30	Same as projectile	7.30	2.643	1	2.17	32.62	14	◇
0.2-in. dia. sphere, 0.0620, 0.50, & 0.22-in. dia. spheres & 0.22-in. dia. (L/D) = 1 cylinder.	AISI 1030 steel; cold rolled steel having a carbon range from 0.12 to 0.30 and a manganese range from 0.30 to 0.60	7.83	Same as projectile	7.83	5.126	1	1.94	30.41	7,13	△
1/8 & 3/16-in. dia. spheres	Iron	7.87	Same as projectile	7.87	5.196	1	--	26.22	17	--
0.375, 0.500, 0.625, & 1.000 in. dia. (L/D) = 0.267, 0.08 & 0.14, 0.72, & 0.064 & 0.10 cylinders.	Steel	7.83	Cadmium	8.65	2.307	0.905	1.74	18.44	5	◺
0.125 & 0.4-in. dia. spheres; 0.0620 & 0.22-in. dia. spheres & 0.22 & 0.50-in. dia. (L/D) = 1 cylinders.	2024-T4 Aluminum; 2024-T3 Aluminum	2.77	Copper	8.96	3.557	0.309	1.12	6.22	7,13	◺
0.375, 0.500, 0.625, & 1.000-in. dia. (L/D) = 0.267, 0.08 & 0.14, 0.72, & 0.064 & 0.10 cylinders; 0.0620 & 0.22-in. dia. spheres & 0.22 & 0.50 in. dia. (L/D) = 1 cylinders	Steel, cold rolled steel having a carbon range from 0.12 to 0.30 and a manganese range from 0.30 to 0.60	7.83	Copper	8.96	3.557	0.874	1.82	24.88	5,13	◺
1/8 & 3/16-in. dia spheres, spheres, 0.22 & 0.50-in. dia. spheres & 0.22 & 0.50-in. dia. (L/D) = 1 cylinders.	Copper	8.96	Same as projectile	8.96	3.557	1	2.03	31.59	17,1,13	◺
0.125 & 0.4-in. dia spheres, 0.0620 & 0.22-in. dia. spheres & 0.22-in. dia. (L/D) = 1 cylinder; 1/4-in. dia spheres	2024-T4 Aluminum, 2024-T3 Aluminum, Aluminum	2.77	Lead	11.34	1.227	0.244	0.89	2.72	7,13,6	◺
0.375, 0.500, 0.625, & 1.000-in dia. (L/D) = 0.267, 0.08 & 0.14, 0.72, & 0.064 & 0.10 cylinders, 0.0620 & 0.22-in. dia spheres & 0.22-in dia (L/D) = 1 cylinder	Steel, cold rolled steel having a carbon range from 0.12 to 0.30 and a manganese range from 0.30 to 0.60	7.83	Lead	11.34	1.227	0.690	1.61	14.60	5,13	◺
0.22 & 0.50-in dia. spheres & 0.22-in dia (L/D) = 1 cylinders	Copper	8.96	Lead	11.34	1.227	0.790	1.96	22.97	13	◺
Spheres 0.22-in. dia spheres & 0.22-in dia (L/D) = 1 cylinders 3/16-in dia spheres	Lead	11.34	Same as projectile	11.34	1.227	1	2.29	38.31	1,13,14	◺